

Micro-orbits in a many-brane model and deviations from Newton's $1/r^2$ law

A. Donini^a, S. G. Marimón

Instituto de Física Corpuscular, CSIC-Universitat de València, Apartado de Correos 22085, 46071 Valencia, Spain

Received: 30 September 2016 / Accepted: 23 November 2016 / Published online: 18 December 2016
© The Author(s) 2016. This article is published with open access at Springerlink.com

Abstract We consider a five-dimensional model with geometry $\mathcal{M} = \mathcal{M}_4 \times \mathcal{S}_1$, with compactification radius R . The Standard Model particles are localized on a brane located at $y = 0$, with identical branes localized at different points in the extra dimension. Objects located on our brane can orbit around objects located on a brane at a distance $d = y/R$, with an orbit and a period significantly different from the standard Newtonian ones. We study the kinematical properties of the orbits, finding that it is possible to distinguish one motion from the other in a large region of the initial conditions parameter space. This is a warm-up to study if a SM-like mass distribution on one (or more) distant brane(s) may represent a possible dark matter candidate. After using the same technique to the study of orbits of objects lying on the same brane ($d = 0$), we apply this method to the detection of generic deviations from the inverse-square Newton law. We propose a possible experimental setup to look for departures from Newtonian motion in the micro-world, finding that an order of magnitude improvement on present bounds can be attained at the 95% CL under reasonable assumptions.

1 Introduction

Even after the discovery of a scalar particle with a mass $m_H = 125.7 \pm 0.4$ GeV [1] in 2012 by the ATLAS and CMS Collaborations (see Refs. [2–8] for recent results), it is well possible that the Standard Model is not the end of the story for several theoretical and experimental reasons. First of all, the Standard Model cannot explain the observed *Dark Matter* component of the Universe energy density, $\Omega_{\text{DM}} \sim 27\%$; it has no clue for the so-called *Dark Energy*, which should determine the observed accelerated expansion of the Universe, $\Omega_{\text{DE}} \sim 0.68\%$; the amount of CP violation in the Standard Model is not enough to explain baryogenesis; and, eventually, the observation of non-vanishing neutrino masses cries

for an extension of the Standard Model that could account for them (allowing, in some extensions, for a baryogenesis-through-leptogenesis scenario). In addition to these experimental hints, the Standard Model does not include gravity, for which a coherent (and unique) quantized theory is lacking. Most of the Standard Model extensions have been advanced to solve some of these problems, by considering it as an effective low-energy theory that should be replaced by a more fundamental one at some scale such as, for example, the Planck scale, $M_P \sim 10^{19}$ GeV. Notice that M_P is well above the electroweak symmetry breaking scale, $\Lambda_{\text{EW}} \sim 246$ GeV, though. This enormous spread sounded *unnatural* [9] for long, generating the so-called *hierarchy problem*. Typical solutions, such as supersymmetry [10] or technicolor [11–13], assume that new physics, responsible for the electroweak symmetry breaking, must be found not much above the electroweak scale. Both hypotheses, however, predict the existence of many new particles not seen up to now at the LHC. A different proposal to solve the hierarchy problem was advanced in the 1990s [14–17]: to explain the large hierarchy between Λ_{EW} and M_P without introducing new physics in between, why do not we lower M_P , instead? This could be done assuming the existence of new spatial dimensions in excess of the observed three ones to which we are used to at human-being length scales. In order for these new dimensions to pass unnoticed to the eye of an observer, they must be compactified in such tiny volumes that direct observation through the measurement of deviations from the inverse-square Newton law for gravitational interactions is beyond the reach of current experiments [18]. If gravity may propagate into the *bulk* $V_n \sim (2\pi R)^n$, with R a generic compactification radius (more complicated compactification schemes may be envisaged), at very small distances compared with R gravity would be D -dimensional (where $D = 4 + n$, n being the number of extra spatial dimensions) with a fundamental scale M_D . On the other hand, at distances much larger than R , gravity behaves as in four-dimensions, with fundamental scale

^a e-mail: donini@ific.uv.es

$M_P^2 \propto (2\pi R)^n M_D^{n+2}$. This relation between M_P and the fundamental scale M_D of a D -dimensional gravitational theory was first derived in Refs. [15, 16, 19]. The relation states that, if V_n is large enough, the fundamental mass scale M_D can be much lower than M_P and, possibly, as low as the electroweak symmetry breaking scale Λ_{EW} , thus solving the hierarchy problem.¹ For $n = 1$, R should be of astrophysical size to have $M_D \sim 1$ TeV. However, for $n \geq 2$ to lower M_D down to some TeV's a sub-mm radius R suffices, something that is not excluded by direct observation of deviations from Newton's $1/r^2$ law: present limits on new spatial dimensions gives $R \leq 44 \mu\text{m}$ at 95% CL for the largest extra dimension compactified in a circle of radius R [20]. A huge literature has been devoted to the study of the virtues and problems of LED models (see, for example, Ref. [21] and references therein), and experimental searches at the LHC of signatures of extra dimensions in high-energy particle scattering are ongoing (see Ref. [1] for a recent update on the LED searches status). Notice, however, that non-observation of the characteristic signatures of LED models at the LHC is pushing limits on M_D well above the TeV scale, thus making them less appealing as an elegant solution to the hierarchy problem.

On the other hand, extra dimensions may be motivated on their own as a possible framework for Dark Matter. In LED models, the Standard Model is added to gravity by introducing two separate terms in the action [22], $S = S_{\text{gravity}} + S_{\text{SM}}$. Whilst S_{gravity} is the D -dimensional Einstein–Hilbert action, S_{SM} is the standard four-dimensional action of the Standard Model. The SM fields are stuck onto a four-dimensional surface called *brane*, a concept borrowed by string theory [23]. Little has been said about an interesting possibility: if we may conceive a space-time in which Standard Model particles are bounded to live on a four-dimensional surface embedded in a higher-dimensional bulk, what forbids the existence of other identical branes, with identical (or different) matter located on them? This hypothesis has not been studied in full detail after having been advanced at the very beginning of the LED proposal at the end of the '90s (albeit, to our knowledge, not in scientific publications). In particular, little interest has been devoted to the possibility that SM-like matter located on a different brane at a distance $|y| < 2\pi|R|$ from us in the extra dimensions may represent a fraction (or the total) of the Dark Matter component in the Universe. Notice that, for three-dimensional distances r much larger than the compactification scale R , $r \gg R$, gravity behaves effectively as in four-dimensions. Therefore, the extra matter located on different branes act identically to standard matter in our Universe, albeit only gravitationally, as gauge interactions are only allowed on directions longitudinal to the

branes, and not transverse to them. The extra matter on other branes, therefore, behaves exactly as Dark Matter (taking into account present bounds on direct and indirect Dark Matter searches, from which only very tight upper bounds on non-gravitational cross-sections of Dark Matter particles with SM ones can be derived, see for example Ref. [24] for a recent review).

Several papers have dealt with similar ideas. For example, in Ref. [25], the idea that the brane in which we live may be folded many times in a small compact volume was pursued. If two foldings of the brane happen to be very near at some point in the extra dimensions, matter located on them would interact gravitationally but not through gauge interactions (whose messengers should travel much longer than gravity), thus behaving as Dark Matter. The same would happen within the framework of what is known as *mirror matter*: matter identical to SM matter, albeit forbidden to interact through gauge fields with SM particles because of a conserved parity number (see, e.g., Ref. [26] and the references therein). In both cases, SM-like matter can interact gravitationally with matter in our Universe but not through other interactions. A lot of work has been devoted to these ideas, trying to fulfill all present cosmological and astrophysical bounds on the Dark Matter properties (see, for example, Refs. [27–30] for the case of mirror matter). One of the main problems for SM-like matter to represent the Dark Matter component of the Universe is the fact that data favors a non-dissipative, collisionless fluid and not matter that, naively, would cluster and form structures identical to those present in the visible sky (see, for example, the literature on *Double Disk Dark Matter* [31, 32]). Attempts to make models of dissipative dark matter agree with observational data can be found, for example, in Refs. [33–35].

This paper, however, is not the place to perform a comprehensive study of a many-branes model with SM-matter located identically on two or more branes as a possible solution to the Dark Matter abundance problem. We will leave this ambitious program, hopefully, to forthcoming publications. We restrict ourselves to a more limited, albeit inspiring goal: to study the classical kinematical behavior of masses located on two distant (in the compact extra dimension) branes under the effect of the D -dimensional gravitational field. We study the simplest case, one single extra spatial dimension compactified on a circle of radius R , whose size should be within the present bounds given above. For simplicity, we have fixed² $R = 10 \mu\text{m}$. We have chosen the masses of a gravitational source m on a distant brane (*there*) and of a test body m' on our brane (*here*) to values such that the typical three-dimensional distance r varies in the

¹ Being a large compact volume the origin of a large four-dimensional Planck mass, this solution to the hierarchy problem is called *Large Extra-Dimensions* (LED).

² We are aware that this model cannot solve the hierarchy problem (as, for a sub-mm size extra dimension, $M_D \sim 5 \times 10^5$ TeV), which could, however, be solved adding more than one extra dimension.

range $r \in [1, 100] \mu\text{m}$, for which we expect to maximize the possible deviations from Newtonian dynamics. We have then derived the range of angular velocities $\dot{\theta}$ for which the orbit of m' around the projection of m on our brane, \mathbf{x}_0 , are not open trajectories. For this choice of initial conditions, we expect from Newtonian gravity stable, periodic, elliptical orbits of m' around \mathbf{x}_0 , \mathbf{x}_0 being one of the foci of the ellipse. On the contrary, we have found that the trajectory of m' around \mathbf{x}_0 in a two-brane five-dimensional model may be either an open path or a bounded one, but cannot be a closed orbit. Bounded orbits are generally not elliptical, not periodic and with revolution times that can change significantly from one revolution to the next. A significant precession of the “periapsis” (defined as the point for which the distance between m and m' is minimal) is also observed in the considered region of the initial conditions parameter space. In order to assess quantitatively for which particular initial conditions we could distinguish Newtonian dynamics from the two-brane five-dimensional one, we have produced mock data describing some characteristics of the orbit in the latter model. For this study, we computed the distance at the periapsis and the “apoapsis” (the point for which the distance between m and m' reaches a maximum) of m' from \mathbf{x}_0 and the time needed for m' to perform the first 2π -revolution around \mathbf{x}_0 (of course, a more complete study of the geometrical shape of the orbit on a time span larger than a single revolution may be done). We have then tried to fit the data using Newtonian dynamics (seeing if the orbit can be indeed described by an ellipse with a focus at \mathbf{x}_0 where a four-dimensional gravitational source of mass M , not necessarily identical to m , lies). Our conclusion is that, in a *gedanken experiment* in which a mass m' is orbiting around “nothing” at \mathbf{x}_0 (i.e. around the projection of m on our brane), the measurement of a few of the geometrical and kinematical properties of the orbit is enough to distinguish the two models in a significant portion of the parameter space (depending, of course, on the distance $d = y/R$ of the two branes: the nearer, the more difficult the two models are to be distinguished). We have found that the most important experimental information (apart from the observation of a precession of the periapsis) is the measurement of the time needed to m' to perform a 2π -revolution around the projection of m . Of course, as long as only two objects are considered, the presence or not of other branes in the extra dimension in addition to the two branes where the two bodies lie is irrelevant, as long as branes are transparent to gravity (see, however, Ref. [36]). However, our analysis could be straightforwardly extended to the case of several objects located on several different branes (i.e. in a truly *many-branes* model) taking into account that the potential acting on m' is just the sum of the potentials originating from n sources m_i ($i = 1, \dots, n$) located at distance $\sqrt{r_i^2 + y_i^2}$ from m' .

Armed with the expertise acquired in the case in which m and m' are located onto different branes, we have applied the same technique to the interesting case $d = 0$, i.e. the case in which the two masses are on the same brane. In other words, may the measurement of the kinematical properties of the orbit of a mass m' around a gravitational field source m in the micro-world be used to detect deviations from the $1/r^2$ Newton’s law? The answer, apparently, is yes. Consider a “planet” P of mass $m \sim 10^{-7}$ g and a “satellite” S with a mass $m' \sim 10^{-9}$ g at a distance from P $r_0 = 190 \mu\text{m}$ with an angular velocity $\dot{\theta}_0 = 1.8 \times 10^{-4}$ rad/s. The Newtonian orbit traveled by S around P has an apoapsis at the starting distance r_0 and a periapsis after half a revolution at a distance $\sim 40 \mu\text{m}$. The period of a 2π -revolution of S around P, with the initial conditions given above is $T_N \sim 7000$ s, i.e. approximately two hours! On the other hand, we have found that if the two masses are located onto a brane in a five-dimensional space-time with an extra dimension compactified on a circle of radius $R = 10 \mu\text{m}$, the distance of the periapsis can be less than a half of the Newtonian one. When S approaches its periapsis, the gravitational field is much more intense than in the Newtonian case, and a gravitational slingshot effect is induced on S. For this reason, the orbit is completely different: an almost elliptical orbit is followed by a very short and very fast nearly circular one. This pattern is repeated every time, with the major axis of the almost elliptical section of the orbit precessing around P at the ratio of $\sim \pi/2$ every two revolutions. The time needed for S to orbit around P is non-constant: a revolution with $T_{\text{long}} \sim T_N$ is followed by a second, very fast one, $T_{\text{short}} \ll T_N$ (with T_{short} ranging between 100 to 1000 s). Measuring several revolution times and fit them to a constant (as expected in the Newtonian case) is, therefore, a very powerful tool to discriminate a gravitational potential different from the Newtonian one.

Notice that, as both the source of the gravitational field m and the test mass m' are on our brane, both can be manipulated. Therefore, we are no longer in the realm of a *gedanken experiment*. We have, therefore, applied the method outlined above to the case of a phenomenological modification of the Newtonian potential in the form of a Yukawa correction proportional to $\alpha G_N m m' \exp(-r/\lambda)$, where $\alpha = 2 \cos d$ and $\lambda = R$ in the case of one compact extra dimension (this way to parametrize deviations from Newton’s $1/r^2$ law is standard in the literature). A possible experimental setup that fulfills the basic requirements (even though it should be clearly studied further in all its details) is the following: put a platinum planet P with mass $m_P \sim 10^{-7}$ g and radius $r_P = 10.3 \mu\text{m}$ at the center of a 1 mm^3 laboratory in vacuum; introduce in the laboratory a diamagnetic satellite S with mass $m_S \sim 10^{-9}$ g (for a pyrolytic graphite sphere, $\rho = 2.2 \text{ g/cm}^3$ and $r_S = 4.8 \mu\text{m}$); insert the lab between two magnets with a magnetic field $B \sim 0.5$ T, such that the diamagnetic sphere may levi-

tate to cancel the Earth gravitational field. Once the diamagnetic sphere, at an initial distance from P $r_0 = 190 \mu\text{m}$, is put into motion with an angular velocity $\dot{\theta}_0 = 1.8 \times 10^4 \text{ rad/s}$ (for example by means of photo-irradiation), we can measure the times T_n it takes to S to perform n revolutions around P and compare with the constant Newtonian period T_N expected for this particular choice of initial conditions. In this way, we have been able to derive the attainable exclusion limits at 95% CL, finding that an upper limit of $\lambda < 2 \mu\text{m}$ can be obtained for $\alpha = 2$ (to be compared with the present limit for one extra dimension $R < 44 \mu\text{m}$ at 95% CL). Limits of a few microns can be put down to $\alpha \sim 10^{-3}$ (where as for $\alpha > 10^5$ bounds below $1 \mu\text{m}$ can be obtained). An important comment is that typical backgrounds that limit the sensitivity of experiments that test deviations from the $1/r^2$ law (such as Coulomb, dipolar or Van der Waals electrical forces) are irrelevant in this case as they correct the gravitational force with a $1/r^2$ dependence on the distance of S from P, and therefore, according to Bertrand's theorem, may not induce precession of the orbit (these backgrounds may only modify the constant revolution time T_N and are, therefore, easily taken into account by looking for variations of the revolution time along the orbit). Another important background, the Casimir force between the test sphere and the gravitational source, is negligible as the test sphere is a diamagnetic object and not a conductive metal. We have checked also that general relativity corrections (which go with $1/r^4$ and may cause a precession of the periastron, as in the case of Mercury) are also negligible. In summary, our results are very promising and we plan to investigate further the possibility to use kinematical measurements of orbits of micro-spheres at micro-distances to test Newton's law.

The paper is organized as follows: in Sect. 2 we recall the gravitational potential felt by a body of mass m' at a distance $d = y/R$ in the extra dimension from the source m of the gravitational field (as from Refs. [37,38]); in Sect. 3 we compute the gravitational force acting on m' in the case when m' is located on a brane at a distance d in the extra dimension from the source (this was first done in Ref. [39]); in Sect. 4 we study the motion of m' under the effect of the gravitational field induced by m when the two bodies are on distant branes for masses, distances and angular velocities such that orbits range from tens to hundreds of microns and quantify statistically the region of the initial conditions parameter space for which the orbit can be distinguished from a Newtonian one; in Sect. 5 we apply the same technique to the case when m and m' lie on the same brane; in Sect. 6 we extend our analysis to the study of general deviations from Newton's $1/r^2$ law using the kinematical properties of micro-orbits; eventually, in Sect. 7 we draw our conclusions.

2 Gravitational potential in $\mathcal{M}_4 \times \mathcal{S}_1$

When the original large extra dimensions model was presented in Refs. [16,17], a simple phenomenological potential was derived in the limit of very large standard dimensions $r = |\mathbf{r}|$ with respect to the average compactification radius $R = |\mathbf{R}|$,

$$V_{4+n}(|\mathbf{r}| \gg |\mathbf{R}|) \sim -\frac{m m'}{M_D^{2+n} R^n r} \sim -\frac{m m'}{M_P^2 r}, \quad (1)$$

where m is the source of the gravitational field, m' a test mass and M_P and M_D are the Planck mass and the fundamental scale of gravity in $D = 4 + n$ dimensions, respectively. The last equation establishes a relation between the two scales:

$$M_P^2 \sim M_D^{2+n} R^n, \quad (2)$$

so that the Planck scale can be much higher than the fundamental scale of gravity M_D if the compact volume $V_n \propto R^n$ is large, thus solving the hierarchy problem. In a subsequent paper, Ref. [19], the size of the first order corrections in $|\mathbf{r}|/R$ was also sketched:

$$V_{4+n}(|\mathbf{r}| \gg |\mathbf{R}|) \simeq -\frac{m m'}{M_P^2} \sum_{(k_1, \dots, k_n)} \frac{e^{-2\pi L|k|/r}}{r}. \quad (3)$$

A complete computation of the gravitational potential in the case of $\mathcal{M}_4 \times \mathcal{S}_n$, however, was only given in Refs. [37,38]. A very simple derivation of the potential can be found in Ref. [39] and it is outlined below for the case at hand of one compact extra dimension, only.

Consider, first, the gravitational potential generated by the mass m in five non-compact dimensions acting on the test mass, m' :

$$V_5^{\text{non-compact}}(r, y) = -\frac{G_5 m m'}{2} \frac{1}{[r^2 + y^2]}, \quad (4)$$

where $l_0 = \sqrt{r^2 + y^2}$ is the distance from the source of the potential, divided into its three-dimensional projection $r = |\mathbf{r}|$ and its extra dimensional component, y . The five-dimensional Newton constant, G_5 is defined as $G_5 \equiv M_D^{-3}$, M_D being the fundamental scale of gravity.

Notice, however, that if we consider now an extra dimension compactified on a circle of radius R , the path of length l_0 is not the only one that connects the mass m' with m : we can reach the source of the potential by traveling along a straight line *wrapping* around the compact dimension as many times as we want. The length of a path that goes k times around the compact dimension is $l_k = \sqrt{r^2 + (y - 2\pi Rk)^2}$. Therefore, the source is effectively *felt* by the mass m' infinitely many times, albeit the gravitational potential is increasingly

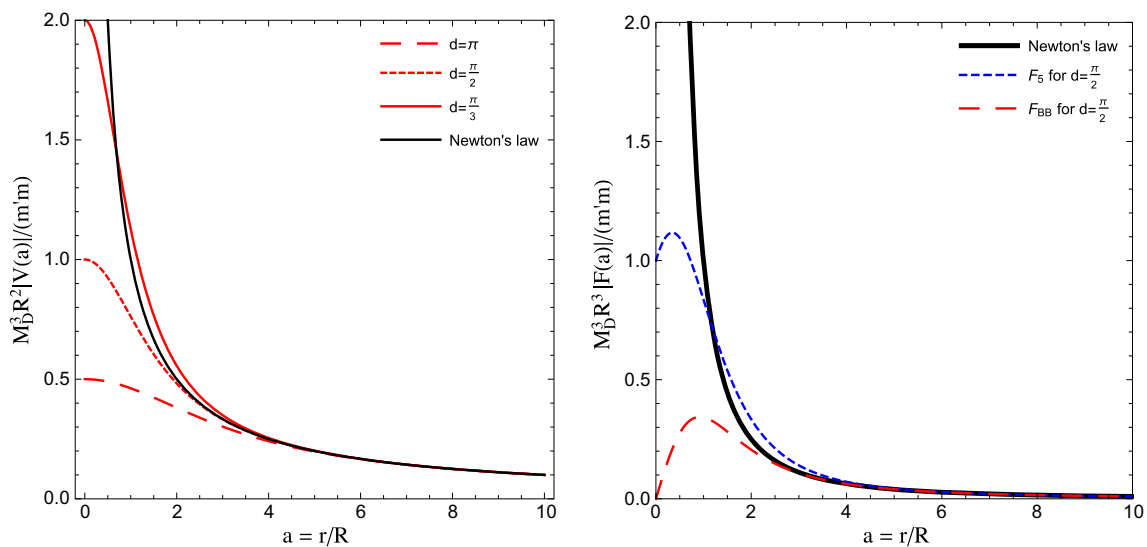


Fig. 1 Left panel the dependence of the five-dimensional potential $V_5^{\text{compact}}(r, y)$ on the three-dimensional distance $a = r/R$ for three different values of $d = y/R$, $d = \pi/3$ (red dashed line), $d = \pi/2$ (red dotted line) and $d = \pi$ (red solid line), for $R = 10 \mu\text{m}$. The Newton potential is plotted with a black solid line as a reference. Right panel

comparison of the different forces: the four-dimensional Newton force (black solid line), the five-dimensional gravitational force $|F_5(a, d)|$ (blue dashed line) and the brane-to-brane force $|F_{\text{BB}}(a, d)|$ (red dotted line), for $d = \pi/2$. All forces are properly rescaled in the vertical axis so as to be comparable in non-dimensional units

feebler as long as we turn more and more. In order to compute the full gravitational potential felt by m' in a compact space-time, we can imagine an infinite extra dimension y with an infinite number of sources m located at distance $2\pi R$ from each other, and just sum their potentials:

$$V_5^{\text{compact}}(r, y) = -\frac{G_5 m m'}{2} \sum_{k=-\infty}^{\infty} \frac{1}{[r^2 + (y - 2\pi Rk)^2]}, \quad (5)$$

where the sum goes from $-\infty$ to $+\infty$ since we can wrap around the compact dimension traveling in both directions. Define $L = 2\pi R$ the length of the compact dimension. Then we use the following identity:

$$\frac{1}{r^2 + (y - Lk)^2} = \frac{1}{2iLr} \left(\frac{1}{k+z} - \frac{1}{k+z^*} \right), \quad (6)$$

where

$$z = -\frac{y + ir}{L}. \quad (7)$$

The potential can thus be written as

$$V_5^{\text{compact}}(r, y) = -\frac{G_5 m m'}{4iLr} \sum_{k=-\infty}^{\infty} \left(\frac{1}{k+z} - \frac{1}{k+z^*} \right), \quad (8)$$

an expression that can easily be summed since

$$\sum_{k=-\infty}^{\infty} \frac{1}{k+z} = \pi \cot \pi z, \quad (9)$$

and, therefore,

$$V_5^{\text{compact}}(r, y) = -\frac{G_5 m m'}{8iRr} (\cot \pi z - \cot \pi z^*). \quad (10)$$

After some algebraic manipulation, we get

$$V_5^{\text{compact}}(r, y) = -\frac{G_5 m m'}{4Rr} \left[\frac{\sinh\left(\frac{r}{R}\right)}{\cosh\left(\frac{r}{R}\right) - \cos\left(\frac{y}{R}\right)} \right]. \quad (11)$$

The five-dimensional potential $V_5^{\text{compact}}(r, y)$ as a function of the normalized three-dimensional distance $a = r/R$ is shown in Fig. 1 (left) for three different values of the normalized distance in the bulk $d = y/R$: $d = \pi/3$, $\pi/2$ and π (light solid, dotted and dashed lines, respectively). As it can be clearly seen, for $a \gg 1$ the potential does not depend on d and becomes identical to the Newtonian four-dimensional potential (depicted as a bold solid line). On the other hand, when $a \sim 1$, the distance d plays a major role in determining the strength of the potential. A very important point to stress is that, for $y \neq 0$, there is no divergence at $r \rightarrow 0$, as the test mass at $\mathbf{l} = (r, y)$ is not (yet) falling into the potential well located at $\mathbf{l} \rightarrow \mathbf{0}$ but it remains at a safe distance y from it.

The limits of small and large a can easily be computed, albeit making a distinction between the case $y = 0$ and $y \neq 0$. For two masses located on the same brane, $y = 0$, at very

short three-dimensional spatial distance from the source we get

$$V_5^{\text{compact}}(a \ll 1, 0) \sim -\frac{G_5 m m'}{2R^2 a^2} + \mathcal{O}(a), \quad (12)$$

i.e. the non-compact five-dimensional potential of Eq. (4). On the other hand, when $y \neq 0$, the potential is quite different:

$$V_5^{\text{compact}}(a \ll 1, d) \sim -\frac{G_5 m m'}{4R^2(1 - \cos d)} + \mathcal{O}(a), \quad (13)$$

as it is dominated by a volume term depending on the size of the extra dimension. Notice that, since the gravitational force attracts necessarily a body in the bulk toward the source of the potential, considered fixed onto a brane, at some time Eq. (4) must be recovered.

When the projection of the vector \mathbf{l} onto the standard three spatial dimensions r is much larger than the compactification radius R , $a \gg 1$, we have

$$V_5^{\text{compact}}(a \gg 1, d) \sim -\frac{G_5 m m'}{4R^2 a} [1 + 2 \cos d e^{-a} + \dots]. \quad (14)$$

The leading term of Eq. (14) is nothing but the standard Newtonian four-dimensional potential, after identifying:

$$G_4 \equiv \frac{G_5}{4R}. \quad (15)$$

The leading correction, on the other hand, introduces a Yukawa-like potential whose impact can be experimentally tested (see Refs. [18, 20]).

3 Gravitational force in $\mathcal{M}_4 \times \mathcal{S}_1$

From the potential $V_5^{\text{compact}}(r, y)$ it can easily be derived the gravitational force acting on a body of mass m' located in the bulk at distance $l_0 = \sqrt{r^2 + y^2}$ from the source of the gravitational field. We have

$$\begin{aligned} \frac{\mathbf{F}_5}{m'} &= -\frac{1}{m'} \nabla V_5 \\ &= -G_5 m \sum_{k=-\infty}^{\infty} \frac{1}{[r^2 + (y - 2\pi Rk)^2]^{3/2}} \hat{l}_k \\ &= -G_5 m \sum_{k=-\infty}^{\infty} \frac{1}{l_k^3} \hat{l}_k, \end{aligned} \quad (16)$$

where $l_k = \sqrt{r^2 + (y - 2\pi Rk)^2}$ and \hat{l}_k is a unit vector pointing in the direction of the mass m' from the source (which depends on the winding number k).

The gravitational force that acts on a mass m' in the bulk under the effect of a mass m located on a brane has also been computed in Refs. [37, 38]. An interesting consequence of Eq. (16) is that, given enough time, any mass located in the bulk will eventually be attracted toward the mass distribution located on the brane and, therefore, the bulk is necessarily empty. The brane acts, in practice, as a “bulk vacuum-cleaner”. On the other hand, this is not true if a mass is stuck to a second brane, different from the one onto which is located the source of the gravitational field. This case has not been treated in the references above, but it has been studied in Ref. [39], instead.

Consider the mass m' at a distance $l_0 = \sqrt{r^2 + y^2}$ where y is the distance along the fifth-dimension between two parallel branes. Since m' cannot escape its own brane, the gravitational force originating at the location of m is partially canceled. The problem resembles, therefore, that of a mass onto an inclined plane, for which only the component of the force that goes along the plane remains. To compute the component of the brane-to-brane force along the second brane, we must derive the potential along r :

$$\begin{aligned} \frac{\mathbf{F}_{\text{BB}}}{m'} &= -\frac{1}{m'} \nabla \Big|_r V_5 \\ &= -G_5 m \sum_{k=-\infty}^{\infty} \frac{\cos \theta_k}{[r^2 + (y - 2\pi Rk)^2]^{3/2}} \hat{r} \\ &= -G_5 m \sum_{k=-\infty}^{\infty} \frac{r}{l_k^4} \hat{r}, \end{aligned} \quad (17)$$

with θ_k the angle between the vector \mathbf{l}_k and our brane, and \hat{r} the (unique) unit vector along the projection of \hat{l}_k onto our brane. Introducing the normalized coordinates $a = r/R$ and $d = y/R$ we get

$$\mathbf{F}_{\text{BB}} = -\frac{G_5 m m'}{4R^3 a^2} f_{\text{BB}}(a, d) \hat{r}, \quad (18)$$

where

$$f_{\text{BB}}(a, d) = \left[\frac{\sinh a}{(\cosh a - \cos d)} - a \frac{1 - \cosh a \cos d}{(\cosh a - \cos d)^2} \right]. \quad (19)$$

Notice that \mathbf{F}_{BB} is quite different from the well-known four-dimensional Newton force: first of all, it is singular at $a \rightarrow 0$ only for $d = 0$, i.e. when the two masses are on the same brane; on the other hand, for $d \neq 0$, the force vanishes as a goes to zero, since the gravitational attraction felt by m' under the effect of m cancels exactly with the constraint that bounds m' to remain on a brane at distance d from the source. The behavior of $|\mathbf{F}_{\text{BB}}|$ as a function of a is shown in Fig. 1 (right): the black (solid) line represents the four-dimensional Newton force, to be compared with the blue (dashed) line

that represents the five-dimensional force $|F_5(a, d)|$ acting on a particle at a distance $l_0 = R\sqrt{a^2 + d^2}$ from the source for the particular case $d = \pi/2$. On the other hand, the red (dotted) line represents the brane-to-brane force $|F_{BB}(a, d)|$ computed in Eq. (18) acting on a particle at a distance l_0 from the source but bounded to a second brane at a distance d from our brane. First of all notice that both $|F_5(a, d)|$ and $|F_{BB}(a, d)|$ coincides with the four-dimensional Newton force for $a \geq 4$ (i.e. above the present experimental bound on R , as they should). In the region $a \in [1, 4]$ the five-dimensional force $|F_5(a, d)|$ is larger than the four-dimensional Newton force, contrary to the naive expectation that is deduced by applying the Gauss theorem to a non-compact space-time. For $a < 1$ the four-dimensional Newton force eventually becomes larger than its five-dimensional counterpart, diverging for $a \rightarrow 0$ (whereas $|F_5(a \rightarrow 0, d)|$ goes to a constant). The brane-to-brane force $|F_{BB}(a, d)|$ is almost identical to the Newton force for $a \geq 2$, whereas the effect of both compactification and of the second-brane constraint becomes dominant for $a < 1$, eventually making $|F_{BB}(a, d)|$ vanish for $a \rightarrow 0$. Eventually, notice that both the brane-to-brane and the five-dimensional force have a maximum for $a \sim 1$.

The small a limit of the brane-to-brane force is

$$|F_{BB}(a \ll 1, d) \simeq -\frac{G_5 m m'}{12R^3} a \frac{(2 + \cos d)}{(1 - \cos d)^2} + \mathcal{O}(a^3). \quad (20)$$

On the other hand, for $a \gg 1$ we have

$$|F_{BB}(a \gg 1, d) \simeq -\frac{G_5 m m'}{4R^3} \left[\frac{1}{a^2} + 2 \cos d \frac{e^{-a}}{a} + \dots \right], \quad (21)$$

where the first term in the expansion gives the $1/r^2$ four-dimensional Newton's law. Notice that, depending on d F_{BB} may be smaller or larger than the Newtonian four-dimensional force.

Using Eq. (21), an upper bound on the compactification radius has been derived, $R \leq 44 \mu\text{m}$ [1]. The lower bound on the fundamental mass scale M_D can then be derived using Eq. (15): we get $M_D \geq 5.5 \times 10^5 \text{ TeV}$ (well beyond LHC reach). Notice that, even if M_D is much lower than the Planck scale M_P , adding only one extra spatial dimension is not enough to solve the hierarchy problem and bring the fundamental scale of gravity down to the electroweak scale as a huge hierarchy between M_D and Λ_{EW} still exists. On the other hand, for two extra spatial dimensions (for which the experimental bound on R gives $R \leq 37 \mu\text{m}$), the lower bound on M_D becomes $M_D \geq 3.6 \text{ TeV}$, within the reach of LHC. Recent limits put by both ATLAS and CMS using different

signals imply that M_D should be greater than a few TeV (see Ref. [1] and updates).

4 Two bodies on different branes: a *gedanken* experiment

Consider now two bodies located on two different branes at a distance $d = y/R$ in the extra dimension, with R fixed to a value allowed by the present bound, $R = 10 \mu\text{m}$ (we have checked that our results do not change significantly for $R \in [10, 50] \mu\text{m}$, after proper tuning of the initial conditions). For simplicity, we fix the source mass m on a distant brane (i.e. *there*) and the test mass m' onto our brane (i.e. *here*). As a consequence, we cannot interact with the source of the gravitational potential (which is out of our experimental reach), whereas we can manipulate the test mass m' : for example, we can choose its mass, its position and its velocity. The question we want to address is the following: can we distinguish the motion of m' induced by m from a four-dimensional Newtonian motion? Clearly, this experiment is not feasible in practice, as we have no handle to control the source, and for this reason it is a *gedanken* experiment. What we can learn from it, however, is interesting in itself, as we will see that just by simple classical measurements of the geometry and period of the motion of m' onto our brane under the effect of the gravitational force induced by an unseen source is enough to exclude a $1/r^2$ Newtonian force as the cause of such a motion.

As a warm-up, we first consider the case of a linear motion in Sect. 4.1. Eventually, we study the two-dimensional case in Sect. 4.2.

4.1 Linear motion

Consider the mass m in a brane at distance $d = y/R$ in the bulk. The projection of its position onto our brane, \mathbf{x}_0 , is taken to be the origin of a three-dimensional coordinate system, $\mathbf{x}_0 = \mathbf{0}$. The test mass m' is located onto our brane at a position \mathbf{x} , such that the distance in three dimensions between the two masses is $r = |\mathbf{x} - \mathbf{x}_0|$. If we take the mass m' to be at rest or with an initial velocity aligned with the attracting gravitational force $\mathbf{F}_{BB}(r, d)$, the resulting motion will be a linear motion. As there is no massive body located at \mathbf{x}_0 (the source is displaced at a distance d in the extra dimension), the test mass m' will not crash onto m . Quite the contrary, it will proceed in its motion, escaping from the source m' or being bounded in a periodic motion in the proximity of \mathbf{x}_0 depending on the initial conditions.

Reducing the problem to a one-dimensional motion along the line that goes from \mathbf{x} to \mathbf{x}_0 , we must solve

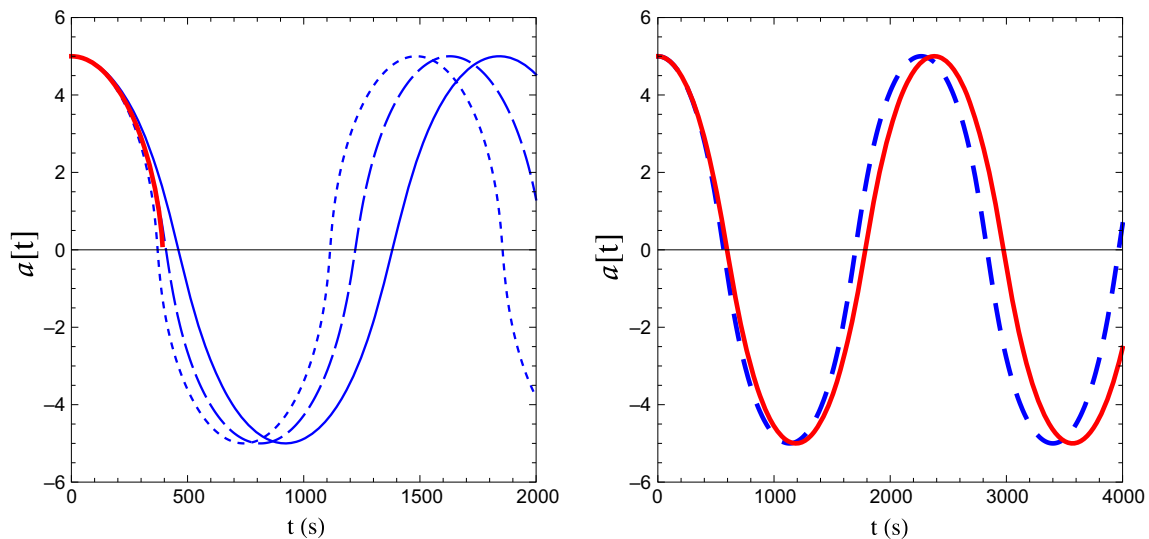


Fig. 2 Normalized distance a between a mass m' and the source of a gravitational field m (or its projection onto our brane, x_0) as a function of time. *Left panel* the red thick line represents $a(t)$ under the effect of a four-dimensional Newtonian force $F_4(a)$; on the other hand, the blue thin lines represent the brane-to-brane motion under the effect of $F_{BB}(a, d)$ for $d = \pi$ (solid blue); $d = \pi/2$ (dashed blue); $d = \pi/4$ (dotted blue). Notice that Newtonian motion ends with a collision of

the two masses in $t \simeq 390$ s. *Right panel* the red solid line represents Newtonian motion for a mass m' constrained on an incline plane at a minimal distance $d = \pi$ from m . The blue dashed line is the brane-to-brane motion under the effect of $F_{BB}(a, \pi)$. In both panel the initial conditions are: $a_0 = 5$ (i.e. $r_0 = 50 \mu\text{m}$) and $\dot{a}_0 = 0$. In the left panel, $k = k_5$ trivially due to Eq. (15). In the right panel, we have fixed $F_4(a, \pi) \equiv F_{BB}(a, \pi)$

$$\ddot{r} = \frac{F(r)}{m'}, \quad (22)$$

where $F(r)$ is either $F_4(r)$ in the case of a four-dimensional Newton force or $F_{BB}(r, d)$ in the case of a brane-to-brane force between particles on branes at distance d in the extra dimension. In the first case, we have

$$\ddot{r}(t) + \frac{G_4 m}{r^2(t)} = 0. \quad (23)$$

For simplicity, we will consider the mass m' small enough to neglect the motion of m under the effect of m' . Let us normalize the distance between the two bodies to the compactification radius R introducing the normalized distance $a = r/R$. The differential equation to be solved is, thus:

$$\ddot{a}(t) + \frac{k}{a^2(t)} = 0, \quad (24)$$

where $k = G_4 m/R^3$ is a coefficient with dimensions s^{-2} . Since R is bounded to be below $44 \mu\text{m}$, the distance at which we want to compare the four-dimensional Newtonian motion with the brane-to-brane case is $r \in [1, 100] \mu\text{m}$. If we choose a mass $m \sim 10^{-7}$ g, then $G_4 m \sim 1 \mu\text{m}^3/\text{s}^2$ (i.e. $k \sim 10^{-3} s^{-2}$) and a is naturally of the required order.

If the two bodies are on different branes, we have

$$a\ddot{a}(t) + \frac{k_5}{a^2(t)} f_{BB}(a, d) = 0, \quad (25)$$

where $k_5 = G_5 m/4R^4$ (using the asymptotic relation in Eq. (15) we have, trivially, $k_5 = G_4 m/R^3 = k$).

In Fig. 2 we show the time evolution of the position a of a body of mass m' under the effect of the gravitational force induced by a body of mass m located at the origin of our three-dimensional coordinate system for the two cases in which the two bodies obey the four-dimensional Newton's law (in red) or the brane-to-brane force $F_{BB}(a, d)$ (in blue). We start at a distance $a_0 = 5$, i.e. $r = 50 \mu\text{m}$, and an initial velocity $\dot{a}_0 = 0$ in both cases. The initial distance is large enough for the four-dimensional Newtonian force to be a good starting approximation (the couplings k and k_5 are taken to be identical). However, under the effect of the gravitational force, we see in the left panel of Fig. 2 that the time evolution changes significantly. The four-dimensional motion (thick red line) approaches $a = 0$ and stops in $t \simeq 390$ s, when the two bodies collide. On the other hand, the brane-to-brane motion reaches $a = 0$ and proceeds until $a = -a_0$ only to turn back and behave periodically like a pendulum. The period of the brane-to-brane motion depends on the distance of the two branes. We show three cases: $d = \pi$ (solid blue), $d = \pi/2$ (dashed blue) and $d = \pi/4$ (dotted blue), for which the period is $T \sim 1800$ s, ~ 1600 s and ~ 1500 s, respectively. Notice that the four-dimensional motion follows the dashed blue line (corresponding to $d = \pi/2$) until crashing. This is a consequence of the particular shape of the brane-to-brane force: in Fig. 1 (right panel) we can see that for $d = \pi/2$ the brane-to-brane force is equivalent to the four-dimensional

Newton force down to distances of $a \sim 2$. On the other hand, for d smaller the brane-to-brane force approaches the five-dimensional force, which in that range of a is stronger than the four-dimensional one (and, thus, the resulting motion is faster). For $d > \pi/2$ we have a slower motion, instead. In the right panel we show a slightly different situation: we consider the four-dimensional Newtonian motion of a mass m' located on an inclined plane at minimal distance $d = \pi$ for the source m of the gravitational field (red, solid line), and compare it with the motion of m' under the effect of the brane-to-brane force induced by a source m on a brane at a distance $d = \pi$ from our brane (blue, dashed line). The five-dimensional coupling k_5 has been tuned such that the strength of $F_{\text{BB}}(a, d) \equiv F_4(a, d)$. We can see that the two motions are both periodic and that the brane-to-brane motion is faster than the four-dimensional motion, with a difference in the period of $\mathcal{O}(100)$ s.

4.2 Orbital motion

It is now time to study the far more interesting case of two-dimensional motion. In this case, again, we can have open trajectories or orbits depending on the initial conditions. We will focus on the latter case, in which the mass m at the source, the initial position and the initial angular velocity of the mass m' are tuned such that a bounded orbit of m' around m (or, more precisely, its projection onto our brane \mathbf{x}_0) is observed.

Let us revise first the Newtonian case, where the equation of motion can be written as

$$m'\ddot{\mathbf{r}} = \mathbf{F}_4(\mathbf{r}) = -\nabla V(r) = -\frac{G_4 m m'}{r^3} \mathbf{r}, \quad (26)$$

where $V(r)$ is the potential energy due to the gravitational field. The total energy is

$$\mathcal{E} = T + V = m' \left\{ \frac{|\mathbf{v}|^2}{2} - \frac{G_4 m}{r} \right\}, \quad (27)$$

where T is the kinetic energy of m' . Writing the velocity in radial coordinates, we have

$$\mathbf{v} = \dot{r} \mathbf{e}_r + r\dot{\theta} \mathbf{e}_\theta, \quad (28)$$

where $(\mathbf{e}_r, \mathbf{e}_\theta)$ are two unit, orthogonal, vectors that define the position of m' at time t in polar coordinates. Expressed in Cartesian coordinates, $\mathbf{e}_r = (\cos \theta, \sin \theta)$ and $\mathbf{e}_\theta = (-\sin \theta, \cos \theta)$. In this basis, the acceleration becomes

$$\dot{\mathbf{v}} = (\ddot{r} - r\dot{\theta}^2) \mathbf{e}_r + (r\ddot{\theta} + 2\dot{r}\dot{\theta}) \mathbf{e}_\theta. \quad (29)$$

It is now trivial to write a system of equations of motion for the mass m' in polar coordinates:

$$\begin{cases} \ddot{r} - r\dot{\theta}^2 = -\frac{G_4 m}{r^2} \\ r\ddot{\theta} + 2\dot{r}\dot{\theta} = 0 \end{cases} \longrightarrow \begin{cases} \ddot{a} - a\dot{\theta}^2 = -\frac{k}{a^2}, \\ a\ddot{\theta} + 2\dot{a}\dot{\theta} = 0, \end{cases} \quad (30)$$

where we have introduced the non-dimensional length $a = r/R$ and k has been defined as in the previous section.

If we now replace the Newtonian four-dimensional force with the brane-to-brane force we have

$$\begin{cases} \ddot{a} - a\dot{\theta}^2 = -\frac{k_5}{a^2} f_{\text{BB}}(a, d), \\ a\ddot{\theta} + 2\dot{a}\dot{\theta} = 0, \end{cases} \quad (31)$$

The second equation implies conservation of angular momentum both for a Newtonian or a brane-to-brane force,

$$h(t) = r^2(t) \dot{\theta}(t) = h_0, \quad (32)$$

where h_0 is a constant of motion. Using this result, the radial equation can be written as

$$\ddot{a} - \frac{h_0^2}{a^3} = \begin{cases} -\frac{k}{a^2}, \\ -\frac{k_5}{a^2} f_{\text{BB}}(a, d), \end{cases} \quad (33)$$

for the Newtonian (above) and brane-to-brane (below) cases, respectively. We get different results in the two cases: for the Newtonian case, solutions of the first of Eq. (30) are conic sections. Possible trajectories are then hyperbolic, parabolic or elliptic. In all cases, they can be described by a simple function,

$$r(\theta) = \frac{r_c}{1 - e \cos \theta}, \quad (34)$$

where $r_c = h_0^2/G_4 m$ and the eccentricity e is given by

$$e = \frac{r_a - r_p}{r_a + r_p}, \quad (35)$$

r_a and r_p being the largest (*apoapsis*) and smallest (*periapsis*) distances of m' from m , respectively. For $e = 0$, $r(\theta)$ describes a circular orbit, whereas for $e < 1$ the orbit is elliptic. For $e \geq 1$ the trajectory is open, being parabolic for $e = 1$ and hyperbolic for $e > 1$. The period of a closed orbit of m' around m can be computed easily applying the third Kepler's law:

$$T_N = \pi \frac{(r_a + r_p)^{3/2}}{\sqrt{2G_4 m}}. \quad (36)$$

The results in the case of a brane-to-brane force are very different. Remember that, according to Bertrand's theorem,

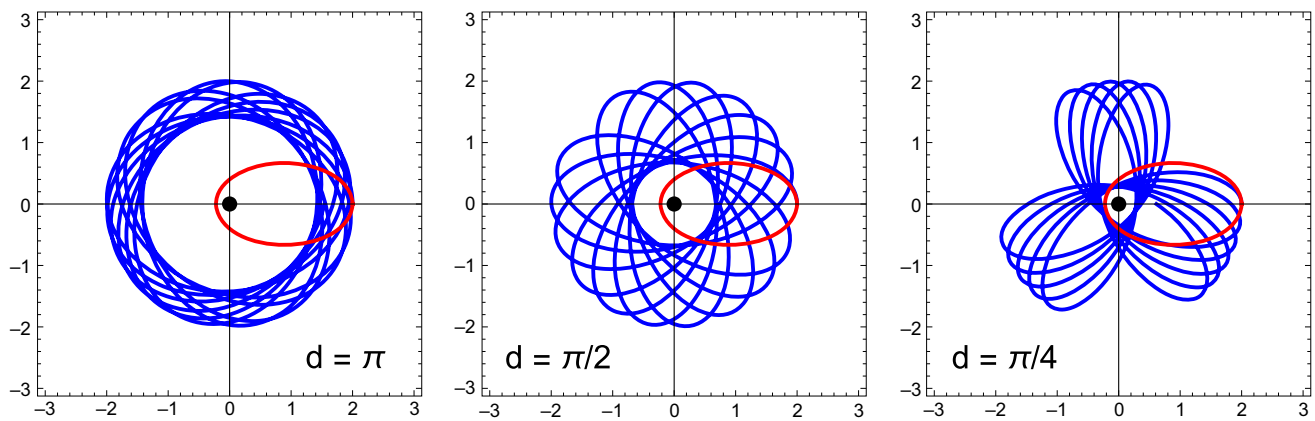


Fig. 3 The trajectory of m' around the source m located at (or whose projection in three dimensions lies at) \mathbf{x}_0 , represented by a black dot. In red, we show the Newtonian elliptic orbit. In blue, we show the motion under the effect of the brane-to-brane force when the two

branes are at a distance $d = \pi$ (left panel), $\pi/2$ (middle panel) and $\pi/4$ (right panel), respectively. The initial conditions are as follows: $k_5 = k = G_4 m / R^3 = 10^{-3} \text{ 1/s}^2$; $a_0 = 2$ ($r_0 = 20 \text{ }\mu\text{m}$); $\dot{\theta}_0 = 5 \times 10^{-3} \text{ rad/s}$

closed orbits are only possible for central forces with a radial dependence of the form $1/r^2$ or r . Any deviation from these two possible functional dependences implies that the resulting orbits are not stable nor closed. A typical example of this is the general relativity correction to the orbit of Mercury: the leading post-Newtonian corrections are of the form $1/r^4$ and induce an observable precession of the perihelion of Mercury. This is precisely the case of the brane-to-brane force: the r -dependence of the (central) force field (either F_5 or F_{BB} , depending if $d = 0$ or not) is not $1/r^2$. As a consequence, we do not expect closed orbits (they may be bounded, though). This is indeed shown in Fig. 3, where we show the trajectory of m' around \mathbf{x}_0 (whose position is represented by a black dot at the origin) for $d = \pi$ (left panel), $\pi/2$ (middle panel) and $\pi/4$ (right panel), respectively. For the brane-to-brane motion, we have plotted (in blue) the first 100 revolutions of m' around \mathbf{x}_0 , only. In all cases, the initial conditions have been chosen such that the Newtonian orbit (depicted in red) is elliptic: $k = G_4 m / R^3 = 10^{-3} \text{ s}^{-2}$; $a_0 = 2$ (i.e. $r_0 = 20 \text{ }\mu\text{m}$); $\dot{a}_0 = 0$; $\dot{\theta}_0 = 5 \times 10^{-3} \text{ rad/s}$ (i.e. $h_0 = 2 \text{ }\mu\text{m}^2 \text{ rad/s}$). The initial angle, θ_0 , can be chosen arbitrarily: we will fix it at $\theta_0 = 0$. Since the initial radial velocity, \dot{a}_0 , is set to be zero, the starting point ($a = a_0, \theta = 0$) is necessarily either the periapsis or the apoapsis of the orbit.

In all panels, we can see a significant precession of the periapsis that induces a rotation of the major axis of the orbit around \mathbf{x}_0 . However, depending on the brane-to-brane distance d , the orbits can be very different even for the same choice of the initial conditions a_0, \dot{a}_0 and $\dot{\theta}_0$. In the left panel of Fig. 3 (corresponding to $d = \pi$), for example, we can see that m' moves along nearly circular orbits with a slow counterclockwise precession of the periapsis. For $d = \pi/2$, orbits are elliptical, instead, whereas precession is still slow as for $d = \pi$. Eventually, for $d = \pi/4$, elliptical orbits are followed by fast nearly circular ones, and precession of the

periapsis is fast, as the major axis rotate of approximately 115° clockwise every two revolutions of m' around \mathbf{x}_0 .

4.3 Distinguishing a brane-to-brane from a Newtonian motion

We want to study now the set of initial conditions for which is possible to distinguish a motion that is compatible with a Newtonian $1/r^2$ force from those that are clearly incompatible with that. To do this, we first compute the region of the parameter space for which we expect m' to orbit around a point. This is easily found computing the minimal angular velocity $\dot{\theta}_0$ for which a particle of mass m' at initial distance r_0 from \mathbf{x}_0 will travel along an open trajectory. This is called the *escape velocity* and it can be computed looking when the kinetic energy exceeds the gravitational potential in Eq. (27), finding

$$\dot{\theta}_0 > \dot{\theta}_{\text{ON}}^{\text{esc}} = \frac{\sqrt{2k}}{a_0^{3/2}} \quad (37)$$

for a Newtonian potential, and

$$\dot{\theta}_0 > \dot{\theta}_{\text{BB}}^{\text{esc}} = \frac{\sqrt{2k_5}}{a_0^{3/2}} \left\{ \frac{\sinh a}{\cosh a - \cos d} \right\}^{1/2} \quad (38)$$

for a brane-to-brane potential, respectively. In order to have an orbit (something that permits to study the geometrical properties of the trajectory over a long period of time) we must thus choose $\dot{\theta}_0$ and a_0 such that they would not violate the escape velocity bound. After checking this condition, we can measure the characteristics of the orbit. Several features distinguish a Newtonian orbit from a non-Newtonian one. We will restrict ourselves in this section to the study of three of them:

- The minimal distance³ from the source of the gravitational field, r_{\min} (i.e. the periapsis r_p for a Newtonian orbit);
- The maximal distance from the source of the gravitational field, r_{\max} (i.e. the apoapsis r_a for a Newtonian orbit);
- The time it takes to m' to make a 2π -revolution around the source of the gravitational field, T_{BB} (i.e. the period T_N computed in Eq. (36) for a Newtonian orbit).

Notice that T_{BB} is a quantity that should be easy to measure experimentally putting an electronic trigger at $\theta = 0$ (e.g. a laser beam can be sent along the $\theta = 0$ direction either to or from the source of the gravitational field, and when m' crosses the beam, thus interrupting it, a signal can be sent to a clock to measure the time lapse). Other possible definitions of T for a non-closed orbit (such as the time it takes to m' , starting at the maximal distance from m , to reach again the maximal distance, for example), are not as easy to measure experimentally and will be therefore discarded. Other geometrical features of the orbit could be used to distinguish the two models: for example, as it will be shown later, the precession of the periapsis is a characteristic feature of non-Newtonian motion. However, without a specific description of the experimental setup used to measure this feature it is not easy to define an observable that can quantify the amount of precession. For this reason, we have restricted ourselves in this section to the limited but sufficient measurement of minimal and maximal distance of m' from x_0 .

Consider now the following *gedanken* experiment: a particle of mass m' onto our brane (*here*) is put into motion around a gravitational source of mass m that is located onto a parallel brane (*there*) at a distance d from our brane. Clearly, we cannot “see” the source of the gravitational potential, as it may emit and absorb photons only in the other brane and it can be felt on our brane only gravitationally (for this reason the experiment is only a *gedanken* experiment). Still, we can put the particle of mass m' into motion with a certain set of initial conditions and measure the characteristics of its orbit. Assume that we know the mass m of the source, the distance d of the two branes and the location of the projection of m onto our brane, x_0 . We can then define a set of possible initial conditions $\{r_0, \dot{r}_0, \dot{\theta}_0\}$. For simplicity, we have chosen $\dot{r}_0 = 0$ throughout our simulation (this is always possible once the position of the projection of m onto our brane is known, as we are assuming, and it corresponds to a particular choice of a coordinate system such that $\dot{r}|_{r_0} = 0, \dot{\theta}|_{r_0} = \dot{\theta}_0$). In our simulation, $k_5 R^3 = G_5 m / 4R = 1 \mu\text{m}^3/\text{s}^2$, corresponding to $m \sim 10^{-7} \text{g}$ and $R = 10 \mu\text{m}$. With this input, the transverse size of orbits is typically in the tens of microns range. We

have considered three possible distances of the two branes: $d = \pi/4, \pi/2$ and π . At this point, we can generate a mock data set including three observables: $\{r_{\min}, r_{\max}, T_{\text{BB}}\}$. The question to ask is: is it possible to reproduce the data with a Newtonian potential? We have performed, therefore, a fit to the mock data using a Newtonian potential with only three free parameters, $\{k, r_{0N}, \dot{\theta}_{0N}\}$, from which the Newtonian observable list $\{r_p, r_a, T_N\}$ can be univocally derived using Eqs. (34) and (36).

As a first step, we have tried to fit the data using only two geometrical information of the orbit, i.e. the minimum and maximum distance of m' from the source of the gravitational field, r_{\min} and r_{\max} . In the case of a Newtonian potential, these two quantities correspond, as we have recalled above, to the periapsis r_p and the apoapsis r_a , respectively. Having only two data points to fit, we have used a two-variable χ^2 :

$$\chi_{2\text{obs}}^2 = \min_{k, r_{0N}, \dot{\theta}_{0N}} \left\{ \frac{[r_p(k, r_{0N}, \dot{\theta}_{0N}) - r_{\min}(k_5, d; r_0, \dot{\theta}_0)]^2}{\sigma_r^2} + \frac{[r_a(k, r_{0N}, \dot{\theta}_{0N}) - r_{\max}(k_5, d; r_0, \dot{\theta}_0)]^2}{\sigma_r^2} \right\}. \quad (39)$$

In the computation of $\chi_{2\text{obs}}^2$ we have assumed that the measurements of the minimum and maximum distance of m' from the source of the gravitational field are Gaussian distributed variables with variance $\sigma_r = 1 \mu\text{m}$. Remember that, for our choice of k_5 , orbits have a typical size of tens of microns. Therefore, the relative error on the measurement of a distance ranges from 10% (for small orbits) to 1% (for large orbits). It is probably possible to measure distances at this length scale with an error better than $1 \mu\text{m}$. However, we consider it a conservative choice. As a second step, we have added the dynamical information regarding the measurement of the period T (defined above). For a Newtonian orbit, this is not an independent variable, as it can be univocally determined using the third Kepler's law knowing r_p, r_a and k . For this reason, adding this piece of information to the fit can be a powerful tool to distinguish between a truly Newtonian orbit and a manifestly non-Newtonian one. In this case, we fit our mock data using a χ^2 with three observables:

$$\chi_{3\text{obs}}^2 = \min_{k, r_{0N}, \dot{\theta}_{0N}} \left\{ \frac{[r_p(k, r_{0N}, \dot{\theta}_{0N}) - r_{\min}(k_5, d; r_0, \dot{\theta}_0)]^2}{\sigma_r^2} + \frac{[r_a(k, r_{0N}, \dot{\theta}_{0N}) - r_{\max}(k_5, d; r_0, \dot{\theta}_0)]^2}{\sigma_r^2} + \frac{[T_N(k, r_{0N}, \dot{\theta}_{0N}) - T_{\text{BB}}(k_5, d; r_0, \dot{\theta}_0)]^2}{\sigma_T^2} \right\}. \quad (40)$$

Also in this case, we assume that the measure of the time required for m' to complete a 2π -revolution around the source of the gravitational field is a Gaussian distributed variable with variance $\sigma_T = 1 \text{s}$. Typical periods T_{BB} in our mock

³ In the simulations and in the plots showing our results, we use as input variable the physical distance r_0 , and not the non-dimensional distance $a_0 = r_0/R$.

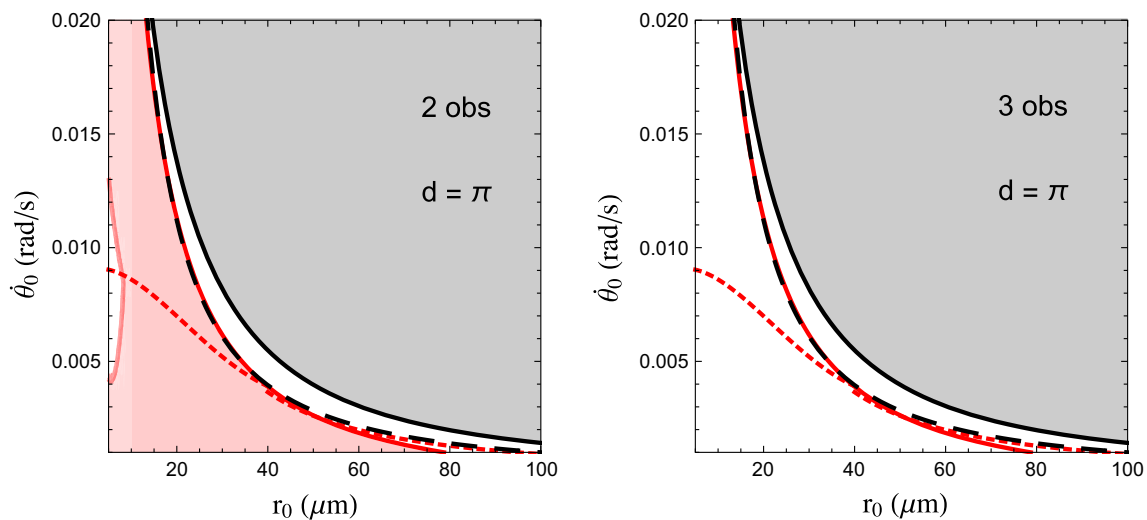


Fig. 4 The p value contour delimiting the region of the $(r_0, \dot{\theta}_0)$ parameter space for which a Newtonian force can or cannot reproduce data corresponding to the orbit of an object of mass m' induced by the gravitational field generated by a mass m located on a brane at distance $d = \pi$. The red-shaded (white) area corresponds to the region for which the p value is above (below) 0.05, i.e. in this region the null hypothesis cannot (can) be rejected. The gray-shaded area corresponds

to the region for which m' “escapes” to the force F_{BB} generated by m . *Left panel* fit performed using measurement of two observables (r_{\min} and r_{\max}), Eq. (39). *Right panel* fit performed using measurement of three observables (r_{\min} , r_{\max} and T), Eq. (40). In both panels, the black dashed line (red dotted line) represents the value of $\dot{\theta}_0$ for which the orbit is circular, $\dot{\theta}_{0,N}^{\text{crit}}$ ($\dot{\theta}_{0,BB}^{\text{crit}}$)

data range from hundreds to thousands of seconds. Therefore, this error on the measurement of a period corresponds to a 0.1–1% error, approximately. Notice that this is a *very* conservative choice, given the state-of-art capability to measure time lapses. However, in most cases it will be enough.

What we are doing here, i.e. fit “experimental” data with a theoretical model asking if the model is able to reproduce the data, is a hypothesis test. The hypothesis **H** that we test is that *data are distributed so as to reproduce some geometrical and dynamical features of a Newtonian orbit* (in statistics, this is called the *null hypothesis*). In order to accept or reject this hypothesis, we adopt the following strategy [1]:

1. We first minimize the χ^2 functions defined in either Eqs. (39) or (40), obtaining χ_{\min}^2 . If the measured observables behave as Gaussian variables, then χ_{\min}^2 is distributed according the χ^2 probability density function, $f(\chi^2, n_d)$, with n_d the number of degrees of freedom.⁴ The χ^2 p.d.f. gives the probability to get a certain value

of χ_{\min}^2 when performing a χ^2 fit to a set of data, given that the data are Gaussian distributed and that the model used to fit the data is correct.

2. We can then compute the p value:

$$p = \int_{\chi_{\min}^2}^{\infty} d\chi^2 f(\chi^2, 1). \quad (41)$$

The p value, as defined above, computes the area of the tail of the χ^2 p.d.f. If p is small, then χ_{\min}^2 is large and the goodness-of-fit is poor (i.e. it is unlikely that rejecting the hypothesis **H** would be a wrong choice). A typical value below which the discrepancy between the hypothesis **H** and the data is considered to be significant is $p = 0.05$.

3. We eventually draw contours for $p = 0.05$ in the $(r_0, \dot{\theta}_0)$ -plane. The results of our hypothesis test are shown in Figs. 4, 5 and 6 for $d = \pi$, $d = \pi/2$ and $d = \pi/4$, respectively.

In all figures, the region of the parameter space for which the fit to data using a Newtonian potential is considered to be good (i.e. where $p > 0.05$) is represented by the light red-shaded area. The region of the parameter space for which we have an open trajectory (i.e. where $\dot{\theta}_0 > \dot{\theta}_{0,BB}^{\text{esc}}$) is gray shaded. Eventually, black dashed and red dotted lines represent the choice of initial conditions for which a Newtonian

⁴ Usually, the number of degrees of freedom of a χ^2 fit is $n_d = N - P$, where N is the number of data points and P the number of fitting variables. However, this is strictly true *only* when the model that we use to fit the data is linear, i.e. $X(\mathbf{n}, \boldsymbol{\theta}) = \theta_1 A_1(\mathbf{n}) + \dots + \theta_P A_P(\mathbf{n})$, where \mathbf{n} ($n = 1, \dots, N$) is the data vector, $\boldsymbol{\theta}$ is the free parameters vector ($\theta = 1, \dots, P$) and $A(\mathbf{n})$ is a basis of functions that depend on the data set. If the functions that form the basis are independent between themselves, then $n_d = N - P$ (otherwise, in general one would get $N - 1 > n_d > N - P$). However, when the model that we use to fit the data is non-linear, n_d cannot be computed straightforwardly (see Ref. [40] and the references therein for some example on this subject). This is, indeed, our case, as Eqs. (34) and (36) imply non-linear relations

Footnote 4 Continued

between the fit parameters r_{0N} , $\dot{\theta}_{0N}$ and k . For this reason, since we want to draw qualitative conclusions on the capability of a Newtonian model to fit data produced by a brane-to-brane force, we will fix $n_d = 1$ in our simulations.

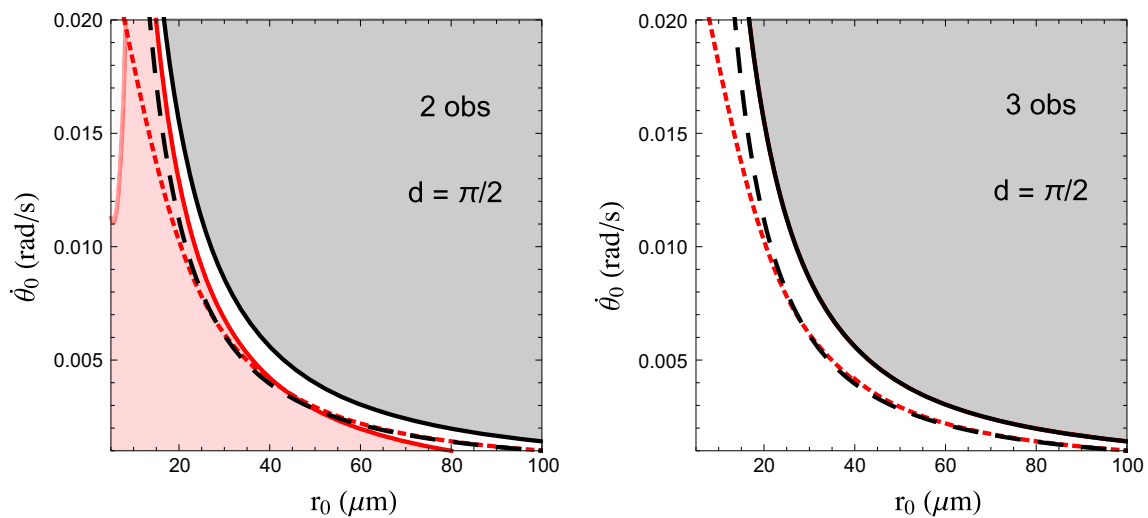


Fig. 5 The same as in Fig. 4 for $d = \pi/2$

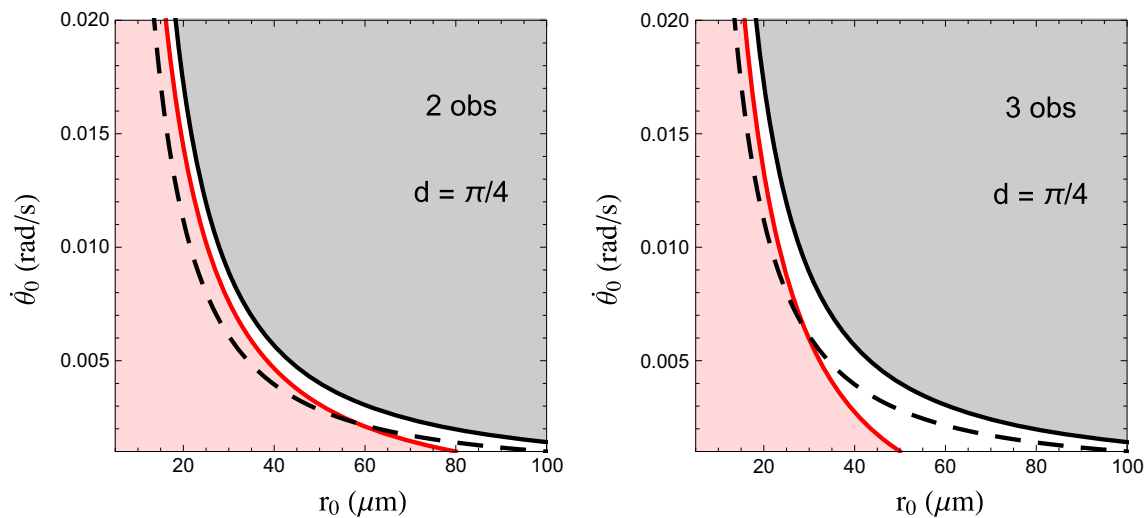


Fig. 6 The same as in Fig. 4 for $d = \pi/4$

(non-Newtonian) orbit is circular (i.e. $r_{\min} = r_{\max}$). Let us call these lines $\dot{\theta}_{0N}^{\text{crit}}$ and $\dot{\theta}_{0BB}^{\text{crit}}$, respectively.

Consider first the case of $d = \pi$, shown in Fig. 4. Using only information from the measurement of r_{\min} and r_{\max} (left panel), the result of a fit to data under the hypothesis that data should reproduce a Newtonian orbit is very good in, approximately, all of the allowed parameter space (i.e. in the region for which we expect a non-open trajectory). There are two regions for which the fit is not good, and therefore rejecting the hypothesis is unlikely to be wrong. The first one is a narrow strip near the bound where trajectories become open. Notice that the gray-shaded area represents the region of the parameter space for which m' escapes to the gravitational force F_{BB} generated by the source m located on a distant brane. For values of the parameters near the escape line, the time needed to make a 2π -revolution becomes longer and the

orbit is very long (as it happens for trans-Plutonian objects in the Solar System). On the other hand, the escape line for a Newtonian force (not plotted) lies within the gray-shaded area, and orbits in the Newtonian case are shorter and faster. For this reason, the fit in this region gives generically a small p value. The second region where the fit is not good corresponds to low r_0 and $\dot{\theta}_0 \sim \dot{\theta}_{0BB}^{\text{crit}}$. This happens since for this particular choice of the input values ($r_0, \dot{\theta}_0$) the data describes a nearly circular orbit (see the left panel of Fig. 3), whereas a Newtonian potential would try to fit them with a hugely elliptical one (as it can be seen looking at the black dashed line, for which $\dot{\theta}_{0N}^{\text{crit}} \gg \dot{\theta}_{0BB}^{\text{crit}}$ for $r_0 \sim R$ and this value of d). Below the red dotted line the BB-orbits are elliptical, too, and the Newtonian model is able to mimic the data. The results are quite different when we introduce information from the measurement of the time required to make a 2π -revolution,

T_{BB} (right panel): in this case, a Newtonian fit to the data gives an extremely small p value in all the parameter space. We conclude that, for $d = \pi$, the measurement of the period with an error $\sigma_T = 1$ s is necessary (and sufficient) to exclude that the observed trajectory is Newtonian.

Consider now the case of $d = \pi/2$, Fig. 5. The fit to two observables (left panel) is very similar to that at $d = \pi$. The only difference is that the critical line $\dot{\theta}_{0,BB}^{crit}$ (red dotted line) is very similar to the Newtonian critical line $\dot{\theta}_{0,N}^{crit}$ (black dashed line) for most of the values of $\dot{\theta}_0$ in the figure; as a consequence, the region for which the fit is bad at low r_0 moves upward (where the difference between the two lines increases). As for $d = \pi$, in the right panel we can see that, after including the measurement of the time needed to make a 2π -revolution, the Newtonian fit is able to reproduce the data in all of the considered region of the initial conditions parameter space.

Consider, eventually, the case of $d = \pi/4$, Fig. 6. The fit to two observables (left panel) shows that a Newtonian potential is able to fit the mock data in all of the considered parameter space. Notice that, in this case, the brane-to-brane and the Newtonian critical lines $\dot{\theta}_{0,BB}^{crit}$ and $\dot{\theta}_{0,N}^{crit}$ coincide for $\dot{\theta}_0 \in [0.001, 0.020]$ (they start to differ for larger values of $\dot{\theta}_0$). For this reason, no area at low r_0 with a poor fit can be found. Once the measurement of the 2π -revolution time lapse is taken into account, we are still not able to distinguish the two models in most of the parameter space. It is interesting to stress, however, that a region for which a Newtonian fit cannot explain the observed data is found at large r_0 , low $\dot{\theta}_0$. This is in apparent contradiction with Eqs. (14) and (42), from which we can see that, for large r_0 , V_5 should approach a Newtonian potential exponentially. This is because, once an angular momentum is included, in the considered range of r_0 the dynamics induced by a Newtonian force still differs from that induced by F_{BB} (and, thus, $T_{BB} \neq T_N$). Since $\sigma_T = 1$ s, the difference in the revolution times is large enough to invalidate the null hypothesis. On the other hand, for larger values of r_0 we expect that the distinction between the two models be no longer possible.

As a last comment, we have checked that for $d = \pi/4$ it is possible to reject the Newtonian hypothesis in the whole considered parameter space if the error on the measurement of the time needed to perform a 2π -revolution of m' around x_0 is lowered. This can be done using $\sigma_T = 0.1$ s, certainly nothing exceedingly difficult to achieve given the state-of-art electronics.

5 Two bodies on the same brane

We have seen in the previous section that, once the mass m' acquires a small angular velocity, the time needed to perform a 2π -revolution around the projection of the source of the

gravitational field m can differ significantly between a Newtonian and a brane-to-brane motion. This is still true even when the two masses lie onto the same brane, i.e. in the case $d = 0$. For this reason, in this section we will study in more detail this case, that can be of direct relevance to improve the bounds on deviations from Newton's $1/r^2$ law.

The problem we want to study is that of a classical two-body gravitational system with a “planet” P with mass $m \sim 10^{-7}$ g and a “satellite” S with mass $m' \sim 10^{-9}$ g, such that we can neglect the motion of P under the effect of S. As we have seen in the previous section, with this choice of masses, the typical orbit of S around P has a radius of tens to hundreds of microns (depending on the initial position r_0 and on the initial angular velocity $\dot{\theta}_0$). We consider, therefore, a “laboratory” with a size of 1 mm^2 . The source should be made of a compact material, in order to reduce its size: for a spherical iron source of mass $m = 10^{-7}$ g, the radius is $r_P = 14.5 \text{ } \mu\text{m}$; for a platinum source with the same mass, $r_P = 10.3 \text{ } \mu\text{m}$. On the other hand, a satellite S of mass $m' = 10^{-9}$ g has a typical size ranging from 2 to $3 \text{ } \mu\text{m}$, depending on the material.⁵ To get an idea, the ratios of masses and radii of S to P are very similar to the corresponding ratios for the Moon and the Earth. The relative distance between S and P that we are considering, on the other hand, is much shorter than the distance between the Earth and the Moon. The satellite S remains in orbit around the planet P because the range of angular velocity that we are dealing with is much larger than the angular velocity of the Moon around the Earth. The first difference between the $d = 0$ and $d \neq 0$ cases is that the potential diverges when m' approaches the source of the gravitational field. Taking into account the physical size of the source and of the satellite, we must choose the range of the initial conditions so as to avoid a collision between P and S. We consider, therefore, the initial distance between the two bodies larger than in the case $d \neq 0$: $r_0 \in [100, 200] \text{ } \mu\text{m}$. The range of angular velocities such that S does not collide with P and does not escape from it is rather narrow for this choice of r_0 : $\dot{\theta}_0 \in [1.5 \times 10^{-4}, 1.5 \times 10^{-3}] \text{ rad/s}$ (notice that the Moon angular velocity around the Earth is $2.66 \times 10^{-6} \text{ rad/s}$). For a typical choice of initial conditions within the range give above, $r_0 = 190 \text{ } \mu\text{m}$ and $\dot{\theta}_0 = 1.8 \times 10^{-4} \text{ rad/s}$, we get a very eccentric Newtonian orbit, $e = 0.775$, to be compared with the nearly circular Moon–Earth orbit, for which $e = 0.0549$.

As in the previous section, we have performed a statistical analysis of the goodness of a Newtonian fit to mock data produced using the five-dimensional force F_5 . Our results are shown in Fig. 7. Again, the gray-shaded area represents the region for which S escapes the gravitational field of P,

⁵ In principle, to reduce backgrounds due to electrical forces between P and S, the satellite should be an insulator. However, alternative choices could be made, depending on the setup adopted (see e.g. Refs. [41–43]).

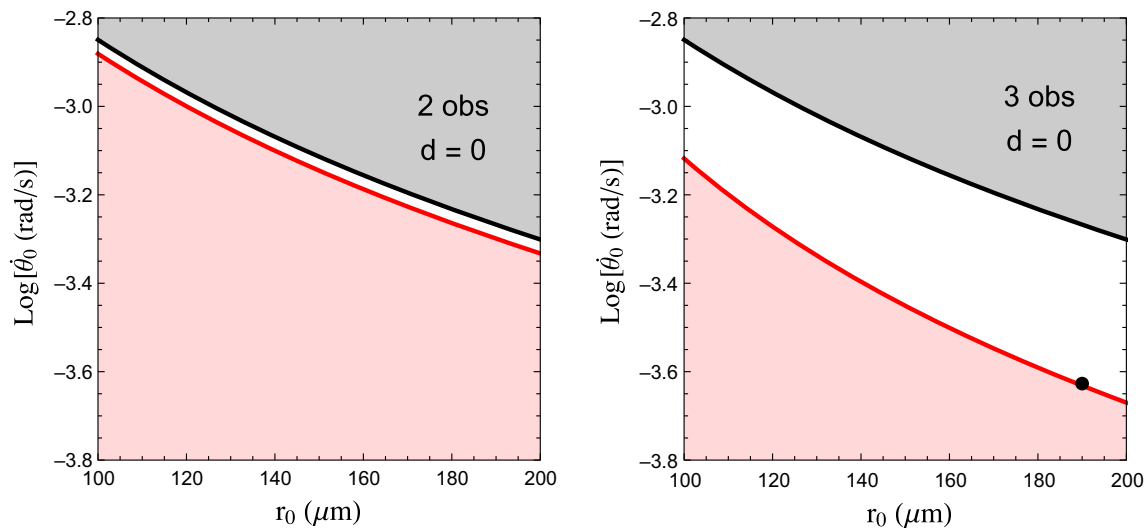


Fig. 7 The p value contour delimiting the region of the $(r_0, \dot{\theta}_0)$ parameter space for which a Newtonian force can or cannot reproduce data corresponding to the orbit of an object of mass m' induced by the gravitational field generated by a mass m located on the same brane (i.e. $d = 0$). The red-shaded (white) area corresponds to the region for which the p value is above (below) 0.05, i.e. in this region the hypothesis cannot (can) be rejected at 95% CL. The gray-shaded area corresponds to the

region for which m' “escapes” to the force F_5 generated by m . *Left panel* fit performed using measurement of two observables (r_{\min} and r_{\max}), Eq. (39). *Right panel* fit performed using measurement of three observables (r_{\min} , r_{\max} and T_5), Eq. (40). The black dot shown in this panel represents the initial conditions choice $r_0 = 190 \mu\text{m}$, $\dot{\theta}_0 = 1.8 \times 10^{-4}$ rad/s discussed below

whereas the light red-shaded area represents the region of the parameter space for which rejecting the Newtonian hypothesis is likely to be wrong (i.e. the region for which $p > 0.05$). The left panel represents a fit to only two observables, r_{\min} and r_{\max} , whereas the right panel includes the information on the time needed for S to perform a 2π -revolution around P, T_5 . In order to present the narrow region of allowed angular velocities, we have shown the vertical axis in logarithmic scale. Notice that, for simplicity, we have considered in our numerical simulations only the case in which the compactification radius is $R = 10 \mu\text{m}$.

As we can see from the right panel of Fig. 7, the information coming from the measurement of the time needed to perform a 2π -revolution of S around P is necessary in order to distinguish the Newtonian orbit from the five-dimensional one. Once this information is included, a white strip in the $(r_0, \dot{\theta}_0)$ -plane for which the distinction is possible emerges. In order to understand better why the two cases give significantly different results, we choose a representative point within the white region of the $(r_0, \dot{\theta}_0)$ -plane and study the main characteristics of the corresponding orbits. Consider then the case of $r_0 = 190 \mu\text{m}$, $\dot{r}_0 = 0$ and $\dot{\theta}_0 = 1.8 \times 10^{-4}$ rad/s, represented by a black dot in Fig. 7 (right panel). The dependence of the distance of S from P as a function of time for the Newtonian and the five-dimensional cases are shown in the left panel of Fig. 8 in red, solid (blue, dashed) lines, respectively. Notice that the plot does not show $t = 0$, for which necessarily r_0 coincides with the apoapsis r_a due to

the initial condition choice. As we can see, the information concerning the distance of S from P is not very inspiring: the maximum distance is always identical for the two cases, whereas the minimum distance of S from P (the periapsis, r_p) is a bit shorter for the five-dimensional case with respect to the Newtonian case. We also notice a rather small shift in the time needed to regain the apoapsis after one revolution. In the right panel of the same figure we present, on the other hand, the gravitational force felt by S under the effect of P along its orbit (multiplied by a convenient factor 10^{22}). We can see that, when S reach its periapsis, the force in the five-dimensional case can indeed be much larger than for the Newtonian case. For the particular choice of r_0 and $\dot{\theta}_0$ given above, we have $F_N(r = r_{p,N}) = 17.3 \times 10^{-22}$ N whereas $F_5(r_{p,5}) = 322.8 \times 10^{-22}$ N, i.e. approximately 20 times larger!

The impressive enhancement of the gravitational force at the periapsis alters completely the orbit of S around P. This is shown in Fig. 9, where the Newtonian orbit is represented as a red, solid line and the first ten (!) revolutions of S around P are shown by blue, dashed line. The black disk at the center of the plot represents the platinum source with a physical size $r_P/R = 1.03$, whereas the satellite is represented by a small black dot starting at a $r_0 = 190 \mu\text{m}$ distance on the positive horizontal axis. Notice that the angular velocity has been fine-tuned so that the five-dimensional orbit never touches the source, i.e. the satellite S never crashes onto the planet P. However, every time that S approaches its periap-

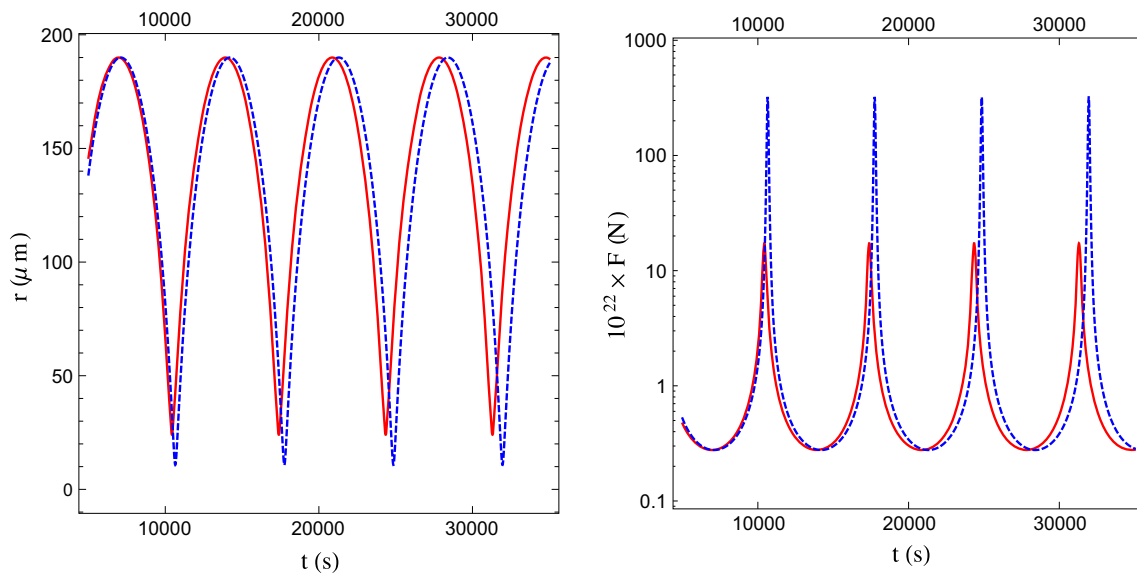


Fig. 8 Distance of S from P and gravitational force at the S position over time for the initial conditions choice $r_0 = 190 \mu\text{m}$ and $\dot{\theta}_0 = 1.8 \times 10^{-4} \text{ rad/s}$. *Left panel* the distance of the satellite S from the planet P as a function of time. *Right panel* the gravitational force

felt by the satellite S under the effect of the planet P as a function of time, multiplied by a factor 10^{22} . In *both panels*, *red solid lines* represent the Newtonian case, whereas *blue dashed lines* represent the five-dimensional case

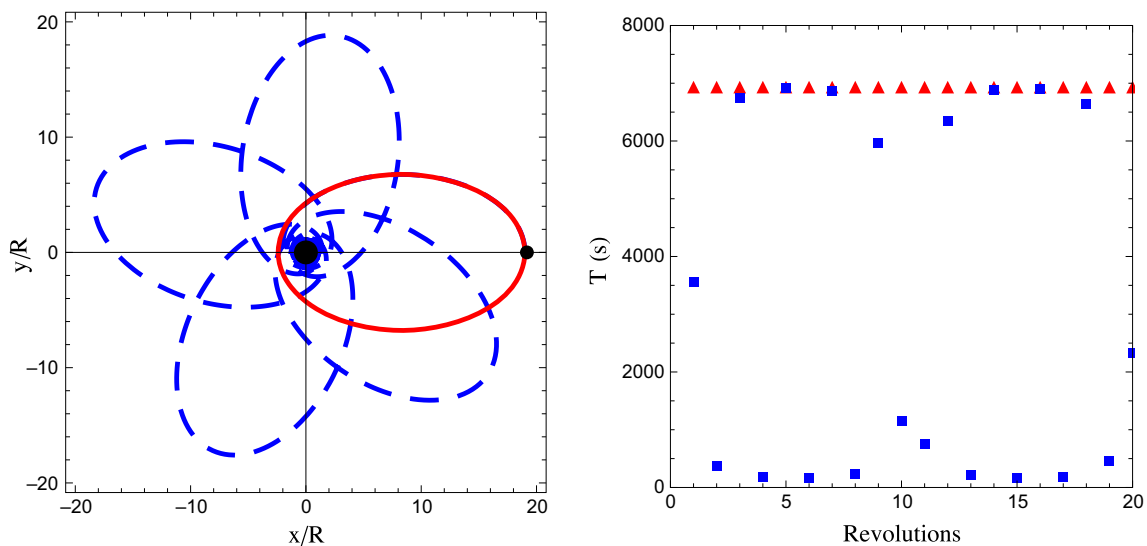


Fig. 9 *Left panel* the orbit of the satellite S (depicted by a black dot at $x_0/R = 19, y_0/R = 0$) around the planet P (at the center of the plot) in the orbit plane for the initial conditions choice $r_0 = 190 \mu\text{m}$ and $\dot{\theta}_0 = 1.8 \times 10^{-4} \text{ rad/s}$. The *red solid line* represents the Newtonian orbit, whereas the *blue dashed line* represents the five-dimensional

orbit. *Right panel* the measurement of the time needed to perform $n 2\pi$ -revolutions of S around P for the same choice of initial conditions. *Red triangles* represent the Newtonian case, whereas *blue squares* represent the five-dimensional case

sis, the source P induces a gravitational slingshot on it, modifying completely its trajectory. The five-dimensional orbit can be described as follows: after a first half-revolution that follows approximately the Newtonian trajectory, the gravitational force of P makes S perform a very fast and short circular orbit around P, only to regain an almost elliptical path that eventually brings it to a new apoapsis, albeit with an approximate 90° shift of the ellipse major axis with respect to the

Newtonian orbit. This pattern: (1) a *long and slow, almost Newtonian, revolution*, followed by (2) a *short and fast, almost circular, one*, repeats until finally regaining (approximately) the initial position after ten revolutions, as shown in the Figure. It is clear that the five-dimensional orbit is geometrically completely different from the Newtonian one. As we will see, the time needed to perform a revolution differs as well.

In the right panel of Fig. 9 we plot the times that S needs to perform a revolution around P . In the Newtonian case, depicted by red triangles, every revolution takes the same time, T_N , which for the particular choice of initial conditions given above is $T_N = 6956.8$ s, i.e. almost two hours! The blue squares represent, on the other hand, the revolution times in the five-dimensional case, T_{5n} , where n stands for the n th 2π -revolution of S around P . In this case, we can appreciate immediately the effect of the gravitational slingshot induced by the huge enhancement of the gravitational force at the periapsis in the five-dimensional case with respect to the Newtonian case: revolution times approximately similar to those computed in the Newtonian case are followed by much shorter revolution times, ranging from ~ 100 to ~ 1000 s. It is this information that can be best used to distinguish the two cases and to improve our present limits on the deviations from Newton's $1/r^2$ law.

6 Deviations from Newton's $1/r^2$ law in four-dimensions

The results obtained in the previous section for the case of gravity in a $\mathcal{M}_4 \times \mathcal{S}_1$ space-time with one extra spatial dimension compactified on a circle of radius R can be generalized to study any deviation from Newton's $1/r^2$ law. Consider the case in which two bodies of mass m and m' , respectively, are located onto our brane (i.e. here). In this case, the gravitational potential generated by m and acting on m' is given by Eq. (11) computed for the special case $y = 0$. When the distance r between the two masses is large compared with the compactification radius (i.e. $a = r/R \gg 1$), the potential can be approximated with Eq. (14). This approximation has the same functional form of the Yukawa potential used to parametrize experimentally deviations from the Newton four-dimensional law:

$$V_{\text{pheno}}(\alpha, \lambda, r) = -\frac{G_4 m m'}{r} \left[1 + \alpha e^{-r/\lambda} \right], \quad (42)$$

with the particular choices $\lambda = R$ and $\alpha = 2 \cos d$ (i.e. $\alpha = 2$ for $d = 0$) and G_4 related to the fundamental five-dimensional coupling by Eq. (15). However, Eq. (42) describes any model⁶ that introduces small, exponentially suppressed, deviations to the inverse-square Newton's law that depend on a single physical scale λ . The yellow (gray for B&W printing) region in Fig. 10 represents bounds at 95% CL on deviations from the four-dimensional Newton's law drawn in the (λ, α) plane (taken from Ref. [18] with bounds obtained in Refs. [20,44–50]). Notice that different theoretical models predict, generically, different expected ranges for

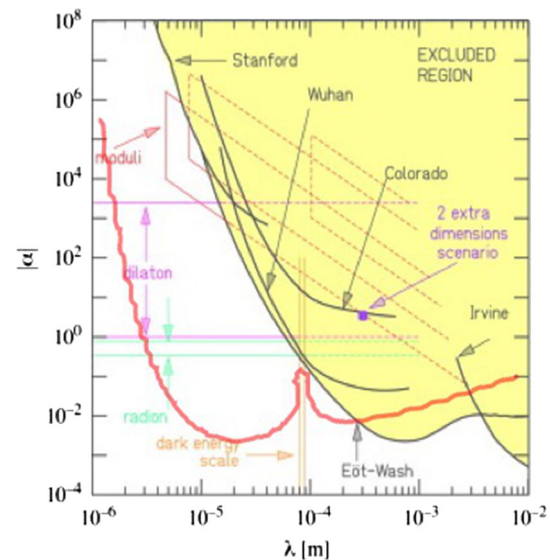


Fig. 10 In yellow, we show the 95% exclusion lines from several experiments on deviations from the four-dimensional $1/r^2$ Newton's law in the (λ, α) plane (from Ref. [18]). These lines correspond to experimental bounds from Refs. [20,44–50]. In red we show the 95% CL bound that can be drawn using the method outlined in this section for a diamagnetic sphere of mass $m' = 10^{-9}$ g put into orbit around a platinum source of mass $m = 10^{-7}$ g with initial distance $r_0 = 190 \mu\text{m}$ and initial angular velocity $\dot{\theta}_0 = 1.8 \times 10^{-4}$ rad/s

α . In the particular case of one compact extra spatial dimension, as we have seen, $\alpha = 2$.

In order to apply the results of Sects. 4 and 5 to study Eq. (42), we sketch the following hypothetical experimental setup:

1. Consider a 1 mm^3 -wide laboratory, with a platinum sphere with radius $r_P = 10.3 \mu\text{m}$ and mass $m_P = 10^{-7}$ g located at the center of the lab.
2. Insert the lab between two magnets, so that we may levitate a diamagnetic satellite in order to cancel the Earth gravitational field;⁷
3. Introduce a diamagnetic sphere with mass $m_S = 10^{-9}$ g in the lab so as to match some carefully chosen initial conditions for its distance from the source and its tangential velocity. The diamagnetic sphere can be, for example, made of pyrolytic graphite, with a density $\rho_{\text{PG}} = 2.2 \text{ g/cm}^3$ (for which the radius of the sphere would be $r_S = 4.8 \mu\text{m}$). In this case, magnets producing a magnetic field $B \sim 0.5 \text{ T}$ suffice to levitate the satellite, given the diamagnetic susceptibility of pyrolytic graphite, $\chi = -16 \times 10^{-5}$ [51,52]. Introducing the satellite into the lab with given initial conditions is, of course, the most difficult task to achieve experimentally. However, recent

⁶ Notice that α may be positive or negative.

⁷ Possible alternatives may be to use an optically cooled levitating dielectric satellite [41–43], or to move the mm^3 -size lab into a zero gravity environment.

results [53] show that levitating pyrolytic graphite may be put into motion by means of photo-irradiation.

Once the diamagnetic satellite S is put into motion around the platinum planet P, we connect a trigger to a clock in such a way that every time the satellite crosses the line $y = 0$ (at any point on the x axis) the measure of the time needed to S to perform a 2π -revolution around P is taken. The error in the measurement of each T_n is the clock sensitivity, neglecting the delay between the trigger and the clock (remember that we are dealing with revolution times that ranges from minutes to hours). We will consider in the statistical analysis that follows a very conservative $\sigma_T = 1$ s error. The collection of N_{rev} revolution times T_n forms our data sample. Once the data are collected, we try to fit our data within the hypothesis that they reproduce a constant revolution time $T_n = T_N$, T_N being the period of a Newtonian revolution. This is done by computing the following χ^2 :

$$\chi^2 = \sum_{n=1}^{N_{\text{rev}}} \frac{(T_n - T_N)^2}{1}. \quad (43)$$

In the following, we have considered $N_{\text{rev}} = 20$, which would correspond approximately to a couple of days of data taking in the case of Newtonian orbits.

This procedure can be applied to the large extra dimension case discussed above, but it can also be generalized to the case of a phenomenological Yukawa potential as the one given in Eq. (42). In this case, the modified gravitational force is

$$F_{\text{pheno}}(\alpha, \lambda, r) = -\frac{G_4 m m'}{r^2} \left[1 + \alpha \frac{r}{\lambda} e^{-r/\lambda} \right], \quad (44)$$

where $\alpha = 2 \cos d$ and $\lambda = R$ in the case of a brane-to-brane force, Eq. (21).

The results obtained using the setup described above and Eq. (43) for the initial conditions $r_0 = 190 \mu\text{m}$ and $\dot{\theta}_0 = 1.8 \times 10^{-4}$ rad/s are shown in Fig. 10. Present bounds, as already said, are represented by the yellow region, whereas our results at 95% CL are shown by a red thick line. It can be seen that the bound on λ can be pushed down to a few microns for any value of $\alpha \geq 10^{-1}$, whereas we get $\lambda < 10 \mu\text{m}$ for α as low as 5×10^{-3} . Below $\lambda = 1 \mu\text{m}$ we lose sensitivity as the exponential factor in the Yukawa potential $\exp(-r/\lambda)$ rapidly kills the signal (to go beyond this limit, entering into the nano-world, we should change m and m'). For $\lambda > 100 \mu\text{m}$ there is also a reduction in the sensitivity due to the r/λ factor in front of the exponential term in Eq. (44). On the other hand, for the particular choice of initial conditions and masses m_S and m_P , we have maximal sensitivity for λ in the interesting range $\lambda \in [10, 100] \mu\text{m}$. Notice that the sensitivity loss that can be seen for $\lambda \sim 80 \mu\text{m}$ is due to a cancelation between the Yukawa correction

to the gravitational force $-(G_N m_S m_P / r^2) \propto r/\lambda \exp(-r/\lambda)$ and the centripetal force term h_0/r^3 in Eq. (33) for the particular choice of the initial conditions. We have eventually checked that our results are independent on the sign of α .

An important point to stress is that in Eq. (43) we have not included backgrounds nor systematic errors. This has not been due to negligence, though. Even if a more careful study of the possible backgrounds should be performed before implementing the setup proposed here in a real experiment, we have thoroughly checked the principal background sources convincing ourselves that they are indeed irrelevant or negligible (for different reasons). We list them in order of importance:

1. First of all, the most important background that limit the sensitivity of experiment searching for deviations from Newton's $1/r^2$ law is that due to electrostatic forces: these may be Coulombian, dipolar and Van der Waals forces. These forces, for macroscopic objects such those considered in the setup proposed above (our S and P spheres are indeed much bigger than molecular or atomic scales), have a $1/r^2$ dependence on the distance of S from P. Therefore, for Bertrand's theorem, they will only modify the period of the orbit of S around P while still maintaining a closed, elliptical orbit with identical times for any revolution of S around P. Deviations from Newton's law in the form of a Yukawa potential, on the other hand, will induce a non-elliptical orbit and a precession of the periapsis. A χ^2 analysis using Eq. (43), but comparing T_n with the average revolution time $\bar{T} = 1/N_{\text{rev}} \sum_{n=1}^{N_{\text{rev}}} T_n$ and not with the Newtonian period T_N , could easily take into account these backgrounds.
2. Another relevant source of background in experiments testing the $1/r^2$ law is the Casimir force acting between the probe and the source of the gravitational field, which are usually both conductors. The Casimir force for two conducting spheres has a rather involved dependence on the distance r between the spheres (see, for example, Ref. [54]), which, however, goes as $1/r^4$ for small distances. This may potentially induce an observable precession of the periapsis. In our case, however, we use a diamagnetic sphere as the probe, thus reducing significantly any possible Casimir force between the two objects.
3. Impurities in the magnetic field used to levitate the diamagnetic sphere are randomly distributed along the sphere orbit. Therefore, they should reasonably average out without affecting the gravitational effects that alter the revolution times T_n pattern.
4. We have also checked that general relativity effects (similar to those causing the Mercury perihelion precession) are completely negligible in the considered setup.

As a final check, we have parametrized the impact of possible backgrounds in the form of a correction of the Newton force by introducing the following potential:

$$V = -\frac{G_N m_S m_P}{r} \left[1 + \frac{Q_1}{Ra} + \frac{Q_2}{R^2 a^2} + \frac{Q_3}{R^4 a^4} \right] \quad (45)$$

where Q_1 , Q_2 and Q_3 are the (dimensionful) couplings of possible sources of backgrounds in units of the gravitational coupling $G_N m_S m_P$. We have found that, in order to have a significant impact on the geometrical and kinematical properties of the orbit, they must be $Q_1/R > 10^{-1}$, $Q_2/R^2 > 10^{-1}$, and $Q_3/R^4 > 1$ for $R = 10 \mu\text{m}$.

In order to realize such an experiment, of course, also systematic errors should be taken into account. This is not the place, however, where to study their impact on the shown results.

7 Conclusions

This paper, as often occurs, started with a limited goal (to study deviations from Newtonian orbits when dealing with a model in which particles are attached to different branes embedded in a compact $(4+n)$ -dimensional space-time) to evolve along its completion to something potentially more ambitious, i.e. the possibility to detect deviations from Newton's $1/r^2$ law using precisely the study of departures from Newtonian orbits in four-dimensions (regardless of the particular model that may induce these departures). In Sects. 2–4, we develop the formalism needed to study the kinematical characteristics of orbits for two bodies lying on different branes in a $\mathcal{M}_4 \times \mathcal{S}_1$ space-time, with an extra spatial dimension compactified on a circle of radius R . First, we computed the gravitational potential in the considered manifold, as it was done in Refs. [37, 38]. Then we computed the force acting on a mass m' attached to a brane at a distance $d = y/R$ from the source of the gravitational field m located on a brane at $y = 0$. This has been done following the outline of Ref. [39]. Eventually, in Sect. 4 we used these results to study the motion of a mass $m' \sim 10^{-9}$ g lying onto our brane, orbiting around the projection of a gravitational source $m \sim 10^{-7}$ g located on a brane at a distance $d = y/R$ from us, with $R = 10 \mu\text{m}$. The considered masses have been chosen so that Newtonian, elliptical, orbits have a typical size ranging from tens to hundreds of microns, i.e. in a region not yet thoroughly tested experimentally. The compactification radius is just below the present upper bound on the size of an extra spatial dimension. Even if this setup cannot explain the large hierarchy between the electroweak symmetry breaking scale Λ_{ew} and the Planck scale M_P , the hierarchy problem may still be solved assuming that more than one extra dimension exists. We have found several interesting features: first of all, orbits are not elliptical in a significant portion of the

initial conditions parameter space. They may be bounded, but they are not closed (as guaranteed by Bertrand's theorem, since correction to the gravitational force have not a $1/r^2$ dependence on the distance). A significant precession of the periapsis (the point at the minimal distance from the source of the gravitational field) is generally observed. The distance at the periapsis can be smaller or larger than the corresponding distance in the Newtonian case, depending on the initial conditions. In addition to this, the time needed to m' to perform a 2π -revolution around the projection of m onto our brane is usually quite different from the (constant) period found in a Newtonian orbit and it may change from a revolution to the next. Therefore, when mock data are produced within a two-brane models and fitted with a Newtonian model, we have found that the fit is poor in a significant portion of the parameter space, i.e. a Newtonian potential is not able to reproduce the data. This result, of course, depends significantly on the distance between the two branes: the nearer, the more difficult the two models are to be distinguished.

Our results seem to imply that the study of the geometrical and kinematical characteristics of orbits in the micro-world may represent a powerful tool to detect deviations from standard Newtonian dynamics at the micron scale. For this reason, in Sect. 5 we have applied the same technique to the interesting case $d = 0$, i.e. when the gravitational source m and the test mass m' lie on the same four-dimensional manifold embedded in a five-dimensional compact bulk. We have found that significant deviations from Newtonian orbits can be observed also in this case, when a reasonable window in the initial conditions parameter space is considered. In particular, for particular choices of the initial conditions, extremely large departures from elliptical, stable and periodic orbits can be seen. The measurement of the time needed to m' to perform n 2π -revolutions around m gives, therefore, a distinctive, unambiguous signature of modifications of Newton's $1/r^2$ law. In order to generalize our results, in Sect. 6 we have applied the same technique to the phenomenological Yukawa potential commonly adopted when searching for departures from Newton's law. Within this framework, the gravitational potential is modified by an additional term in the form $\alpha G_N m m' \exp(-r/\lambda)$ where, for the particular case of LED, $\alpha = 2n$ (n being the number of extra spatial dimensions) and $\lambda = R$. Typical bounds on λ ranges from $\lambda < 1 \mu\text{m}$ for $\alpha > 10^{10}$ to $\lambda < 100 \mu\text{m}$ for $\alpha \sim 10^{-3}$. In the case $\alpha = 2$ (i.e. in the case of one LED), we have $\lambda < 44 \mu\text{m}$. We have therefore proposed a possible experimental setup that could take advantage of the results of the previous sections and that could be used to improve our present bounds in the (λ, α) -plane. The setup consists of a 10^{-7} g platinum gravitational source at the center of a 1 mm^3 laboratory, inserted between two magnets with a magnetic field $B \sim 0.5 \text{ T}$ so to levitate a 10^{-9} g diamagnetic satellite (in order to cancel the Earth gravitational field). The satellite is put into orbit

around the source at an initial distance $r_0 = 190 \mu\text{m}$ with an angular velocity $\dot{\theta}_0 = 1.8 \times 10^{-4} \text{ rad/s}$ (where the initial conditions are chosen to maximize the distortion of the orbit with respect to a Newtonian one, while avoiding the crash of the satellite onto the planet surface). The resulting orbit is extremely irregular: for $\alpha = 2$, $\lambda = 10 \mu\text{m}$, an almost elliptical, very slow, half orbit is followed by a nearly circular, very fast, one, such that the revolution times change abruptly from one revolution to the next. The significant gravitational slingshot effect is caused by a stronger gravitational force at the periapsis of the orbit. For larger values of α and smaller values of λ , we have found that measuring the first 10–20 revolution times seems to be enough to detect small departures from elliptical, periodic orbits and, thus, from Newton's $1/r^2$ law. Bounds below a few microns on λ can be obtained at 95% CL for $\alpha > 1$, whereas for $\alpha > 5 \times 10^{-3}$ we can put a limit $\lambda < 10 \mu\text{m}$ at the same CL (the present bound on λ for $\alpha = 10^{-2}$ is $\lambda < 300 \mu\text{m}$). Although our statistical analysis has been carried out with no backgrounds, we have checked that the most relevant backgrounds that afflict experiments looking for deviations from Newton's $1/r^2$ law, such as Coulombian, dipolar or Van der Waals forces, Casimir attraction or general relativity corrections, are either irrelevant (as they cannot cause a precession of the periapsis or alter the periodicity of the orbit) or negligible in the considered setup.

We are therefore convinced that further studies regarding the feasibility of the proposed experiment should be carried on in order to determine the viability of this technique, which could improve our present bounds on deviations from Newtonian gravity in the micro-world by an order of magnitude or more.

Acknowledgements We are strongly indebted with A. Cros for discussions regarding some experimental aspects of the paper beyond our expertise. We acknowledge also useful discussions with P. Hernández, O. Mena, C. Peña-Garay, N. Rius and M. Sorel. This work was partially supported by Grants: MINECO/FEDER FPA2012-31686, FPA2014-57816-P, FPA2015-68541-P, PROMETEOII/2014/050 de la Generalitat Valenciana, MINECO's "Centro de Excelencia Severo Ochoa" Programme under Grants SEV-2012-0249 and SEV-2014-0398, and the European projects H2020-MSCA-ITN-2015 674896-ELUSIVES and H2020-MSCA-RISE-2015.

Open Access This article is distributed under the terms of the Creative Commons Attribution 4.0 International License (<http://creativecommons.org/licenses/by/4.0/>), which permits unrestricted use, distribution, and reproduction in any medium, provided you give appropriate credit to the original author(s) and the source, provide a link to the Creative Commons license, and indicate if changes were made. Funded by SCOAP³.

References

- Particle Data Group, K. Olive et al., Chin. Phys. C **38**, 090001 (2014)
- ATLAS Collaboration, G. Aad et al., Phys. Lett. B **726**, 88 (2013). [arXiv:1307.1427](#)
- ATLAS Collaboration, G. Aad et al., Phys. Rev. D **90**, 052004 (2014). [arXiv:1406.3827](#)
- ATLAS Collaboration, G. Aad et al. Phys. Rev. D **91**, 012006 (2015). [arXiv:1408.5191](#)
- ATLAS Collaboration, G. Aad et al., Phys. Rev. D **90**, 112015 (2014). [arXiv:1408.7084](#)
- CMS Collaboration, S. Chatrchyan et al., JHEP **1401**, 096 (2014). [arXiv:1312.1129](#)
- CMS Collaboration, S. Chatrchyan et al., Phys. Rev. D **89**, 092007 (2014). [arXiv:1312.5353](#)
- CMS Collaboration, V. Khachatryan et al., Eur. Phys. J. C **74**, 3076 (2014). [arXiv:1407.0558](#)
- G. 't Hooft, NATO Sci. Ser. B **59**, 135 (1980)
- S. Dimopoulos, H. Georgi, Nucl. Phys. B **193**, 150 (1981)
- S. Weinberg, Phys. Rev. D **13**, 974 (1976)
- S. Weinberg, Phys. Rev. D **19**, 1277 (1979)
- L. Susskind, Phys. Rev. D **20**, 2619 (1979)
- I. Antoniadis, Phys. Lett. B **246**, 377 (1990)
- I. Antoniadis, S. Dimopoulos, G. Dvali, Nucl. Phys. B **516**, 70 (1998). [arXiv:hep-ph/9710204](#)
- N. Arkani-Hamed, S. Dimopoulos, G. Dvali, Phys. Lett. B **429**, 263 (1998). [arXiv:hep-ph/9803315](#)
- I. Antoniadis, N. Arkani-Hamed, S. Dimopoulos, G. Dvali, Phys. Lett. B **436**, 257 (1998). [arXiv:hep-ph/9804398](#)
- E. Adelberger, J. Gundlach, B. Heckel, S. Hoedl, S. Schlamminger, Prog. Part. Nucl. Phys. **62**, 102 (2009)
- N. Arkani-Hamed, S. Dimopoulos, G. Dvali, Phys. Rev. D **59**, 086004 (1999). [arXiv:hep-ph/9807344](#)
- D. Kapner et al., Phys. Rev. Lett. **98**, 021101 (2007). [arXiv:hep-ph/0611184](#)
- E. Ponton, *The Dark Secrets of the Terascale: Proceedings, TASI 2011, Boulder, Colorado, USA, Jun 6–Jul 11, 2011* (2013), pp. 283–374. [arXiv:1207.3827](#)
- R. Sundrum, Phys. Rev. D **59**, 085009 (1999). [arXiv:hep-ph/9805471](#)
- J. Polchinski, 293 (1996). [arXiv:hep-th/9611050](#)
- F.S. Queiroz, (2016). [arXiv:1605.08788](#)
- N. Arkani-Hamed, S. Dimopoulos, G.R. Dvali, N. Kaloper, JHEP **12**, 010 (2000). [arXiv:hep-ph/9911386](#)
- R. Foot, Acta Phys. Polon. B **32**, 2253 (2001). [arXiv:astro-ph/0102294](#)
- AYu. Ignatiev, R.R. Volkas, Phys. Rev. D **68**, 023518 (2003). [arXiv:hep-ph/0304260](#)
- P. Ciarcelluti, Int. J. Mod. Phys. D **14**, 187 (2005). [arXiv:astro-ph/0409630](#)
- P. Ciarcelluti, Int. J. Mod. Phys. D **14**, 223 (2005). [arXiv:astro-ph/0409633](#)
- P. Ciarcelluti, Int. J. Mod. Phys. D **19**, 2151 (2010). [arXiv:1102.5530](#)
- J. Fan, A. Katz, L. Randall, M. Reece, Phys. Dark Univ. **2**, 139 (2013). [arXiv:1303.1521](#)
- M. McCullough, L. Randall, JCAP **1310**, 058 (2013). [arXiv:1307.4095](#)
- R. Foot, S. Vagnozzi, Phys. Rev. D **91**, 023512 (2015). [arXiv:1409.7174](#)
- R. Foot, S. Vagnozzi, Phys. Lett. B **748**, 61 (2015). [arXiv:1412.0762](#)
- R. Foot, S. Vagnozzi, JCAP **1607**, 013 (2016). [arXiv:1602.02467](#)
- M. Carena, T.M.P. Tait, C.E.M. Wagner, Acta Phys. Polon. B **33**, 2355 (2002). [arXiv:hep-ph/0207056](#)
- A. Kehagias, K. Sfetsos, Phys. Lett. B **472**, 39 (2000). [arXiv:hep-ph/9905417](#)
- E. Floratos, G. Leontaris, Phys. Lett. B **465**, 95 (1999). [arXiv:hep-ph/9906238](#)

39. H. Liu (2003). [arXiv:hep-ph/0312200](#)
40. R. Andrae, T. Schulze-Hartung, P. Melchior (2010). [arXiv:1012.3754](#)
41. A.A. Geraci, S.B. Papp, J. Kitching, Phys. Rev. Lett. **105**, 101101 (2010). [arXiv:1006.0261](#)
42. Z.Q. Yin, A.A. Geraci, T. Li, Int. J. Mod. Phys. B **27**, 1330018 (2013). [arXiv:1308.4503](#)
43. A.A. Geraci, H. Goldman, Phys. Rev. D **92**, 062002 (2015). [arXiv:1412.4482](#)
44. C.D. Hoyle, D.J. Kapner, B.R. Heckel, E.G. Adelberger, J.H. Gundlach, U. Schmidt, H.E. Swanson, Phys. Rev. D **70**, 042004 (2004). [arXiv:hep-ph/0405262](#)
45. R. Spero, J.K. Hoskins, R. Newman, J. Pellam, J. Schultz, Phys. Rev. Lett. **44**, 1645 (1980)
46. J.K. Hoskins, R.D. Newman, R. Spero, J. Schultz, Phys. Rev. D **32**, 3084 (1985)
47. L.C. Tu, S.G. Guan, J. Luo, C.G. Shao, L.X. Liu, Phys. Rev. Lett. **98**, 201101 (2007)
48. J.C. Long, H.W. Chan, A.B. Churnside, E.A. Gulbis, M.C.M. Varney, J.C. Price, Nature **421**, 922 (2003)
49. J. Chiaverini, S.J. Smullin, A.A. Geraci, D.M. Weld, A. Kapitulnik, Phys. Rev. Lett. **90**, 151101 (2003). [arXiv:hep-ph/0209325](#)
50. S.J. Smullin, A.A. Geraci, D.M. Weld, J. Chiaverini, S.P. Holmes, A. Kapitulnik, Phys. Rev. D **72**, 122001 (2005). [arXiv:hep-ph/0508204](#) [Erratum: Phys. Rev. D **72**, 129901 (2005)]
51. D.B. Fischbach, Phys. Rev. **123**, 1613 (1961)
52. M.D. Simon, A.K. Geim, J. Appl. Phys. **87**, 2600 (2000)
53. M. Kobayashi, J. Abe, J. Am. Chem. Soc. **134**, 20593 (2012)
54. A. Bulgac, P. Magierski, A. Wirzba, Phys. Rev. D **73**, 025007 (2006). [arXiv:hep-th/0511056](#)